

Faculty of Physics and Astronomy

University of Heidelberg

Diploma thesis
in Physics

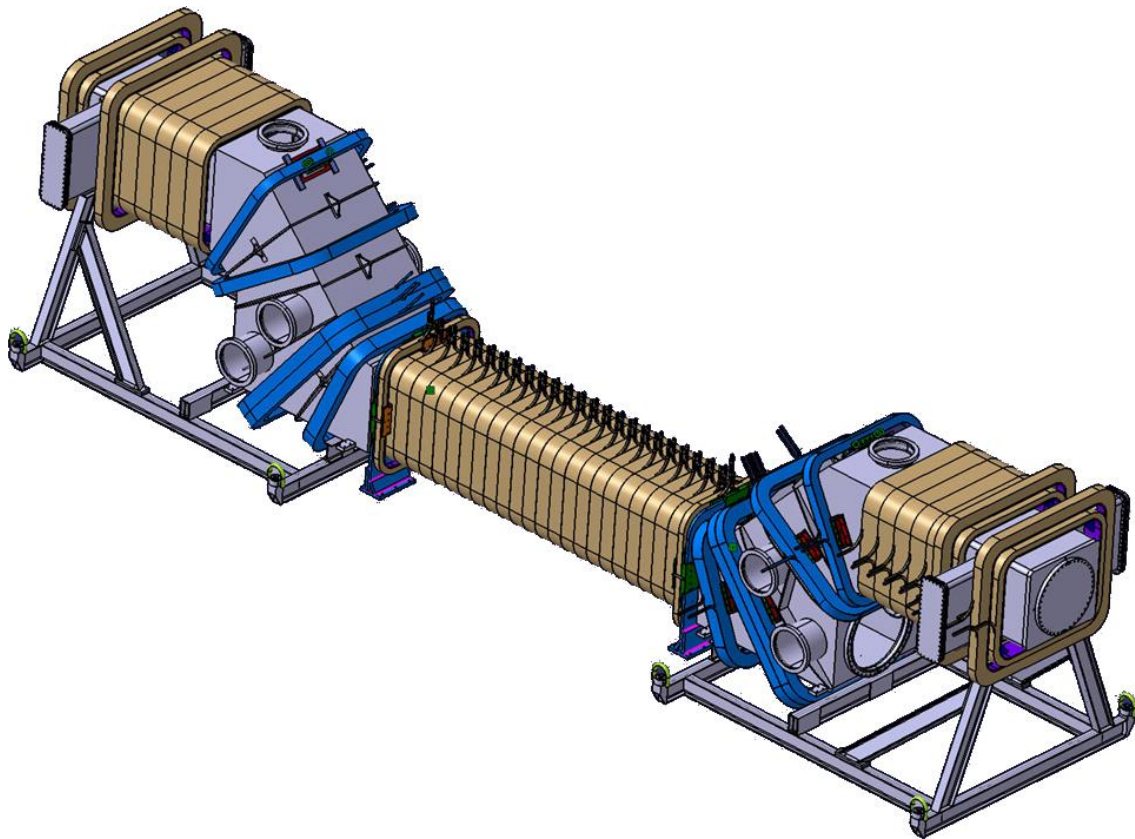
submitted by

Alexander Kaplan

born in Heidelberg

January 2007

Preparing a weak magnetism measurement in free neutron decay with the new spectrometer PERKEO III



This diploma thesis has been carried out by
Alexander Kaplan
at the Physics Institute of the University Heidelberg
under the supervision of
Prof. Dr. Hartmut Abele

Abstract

Preparing a weak magnetism measurement in free neutron decay with the new spectrometer PERKEO III.

We present the preparation of the first measurement with the new spectrometer PERKEO III: The weak magnetism form factor will be obtained from the electron asymmetry A measured in the decay of free polarized neutrons. Previously, this very small energy dependence of A was not accessible due to statistical limits. For the first time ever, PERKEO III provides a neutron decay rate high enough to reach the necessary precision. It is the first of the PERKEO instruments that uses normal conducting coils to produce its magnetic field. To dissipate the heat produced by the power of 283 kW a water cooling system was developed and tested in this thesis. The data acquisition system of the predecessor PERKEO II is reused largely but had to be accelerated: It is now able to cope with 100 times higher data rate. During the first beam time in 2006, the instrument was installed at the cold neutron beam facility PF1b at the Institut Laue-Langevin (ILL) in Grenoble, France. The cooling system was set up and works reliable, the data acquisition system was put into operation, and first measurements were made.

Zusammenfassung

Vorbereitung einer Messung des Schwachen Magnetismus im Zerfall freier Neutronen mit dem neuen Spektrometer PERKEO III

Wir präsentieren die Vorbereitungen der ersten Messung mit dem neuen Spektrometer PERKEO III: Der Formfaktor des Schwachen Magnetismus soll aus einer Messung der Elektron Asymmetrie A im Zerfall freier, polarisierter Neutronen bestimmt werden. Vorher war diese kleine Energieabhängigkeit aus statistischen Gründen nicht zugänglich. Zum ersten Mal überhaupt wird PERKEO III eine Neutronen-Zerfallsrate zur Verfügung stellen, die groß genug ist, um die notwendige Präzision zu erreichen. Es ist das erste PERKEO Instrument mit normalleitenden Spulen, um sein Magnetfeld zu erzeugen. Um die Wärme abzuführen, die von 283 kW Leistung erzeugt wird, wurde im Rahmen dieser Arbeit ein Wasser-Kühlsystem entwickelt und getestet. Das Datenaufnahme-System des Vorgängers PERKEO II wird weitgehend weiterverwendet, musste aber beschleunigt werden: Es kann nun mit den bis zu 100 mal größeren Datenraten umgehen. Während der ersten Strahlzeit 2006 wurde das Instrument am Strahlplatz für kalte Neutronen PF1b am Institut Laue-Langevin (ILL) in Grenoble (Frankreich) aufgebaut. Spulen-Kühlung und Datenaufnahmesystem wurden in Betrieb genommen und arbeiten zuverlässig, und erste Messungen wurden durchgeführt.

Contents

1. Introduction	9
2. Overview	11
2.1. Short Overview of Theory	11
2.2. PERKEO III Overview	12
3. Cooling System	17
3.1. Fundamentals	17
3.2. Cooling Circulations	22
3.3. Waterflow Watchdog	24
3.4. Measurements	26
4. Data Acquisition	29
4.1. Overview	29
4.2. Data Rate Improvement	32
4.3. Dackel	35
4.4. Linearity of ADCs	39
4.5. Photomultiplier Tests	42
5. First Beamtime	47
5.1. Beam Direction	47
5.2. Background Measurements	49
6. Summary	55
A. Time measurement in Linux using the TSC	57

1. Introduction

The free neutron is an ideal object for studies on the structure weak interaction. With its life time of approximate 15 minutes it is the instable particle with the longest life time. Sources of high neutron flux are available, allowing precision measurements with very good statistics. The big advantage of investigating the weak interaction with free neutrons is that no corrections due to nuclear structure are necessary in contrast to the instable elements from the nuclide chart.

Over the past years, the decay of neutrons has been successfully studied by measuring correlation coefficients in experiments with the PERKEO instruments [Abe02, Kre05]. PERKEO III is the latest child in this family of instruments, developed by Bastian Märkisch as topic of his dissertation [Mär06]. It uses the same measuring principle but allows much higher event rates, since it is much larger than its predecessors. Building up the new spectrometer and putting it into operation for a measurement of the weak magnetism coefficient is the topic of this diploma thesis. We obtain the weak magnetism from a small linear dependence of the electron asymmetry in the decay of polarized neutrons. Due to the high statistics necessary to determine such a small coefficient it was not possible to detect it in neutron decay before. The experiment takes place at the high flux cold neutron facility PF1b of the Institute Laue-Langevin (ILL), Grenoble in winter 2006 / 2007.

PERKEO III is the first of the PERKEO instruments that uses normal conducting copper coils to generate its magnetic field. A water cooling system for the coils had to be dimensioned and developed which is presented in chapter 3. With the new experiment we expect a decay rate of approximate 30 kHz what made an acceleration of the existing data acquisition system necessary: One subject of this thesis is the upgrade of the electronics and the development of the new data acquisition software, described in chapter 4. During the first part of the beam time, the instrument was installed and several tests concerning the shielding of background radiation were done. We also examined the influence of adjacent experiments on the background. The results are summarized in chapter 5. We begin with an overview of the theory and the setup of PERKEO III in the next chapter.

2. Overview

In this chapter we give a brief overview on the theory of the neutron decay. In the second part, we present the spectrometer PERKEO III and the setup of the first beamtime. We also show how the measured electron asymmetry A_{exp} is related with the weak magnetism κ .

2.1. Short Overview of Theory

The free neutron decay

$$n \rightarrow p + e^- + \bar{\nu}_e \quad (2.1)$$

can be seen as the prototype of the semi-leptonic weak decay of a baryon. The decay probability $d\omega$ with an electron energy E_e is calculated with Fermi's Golden Rule

$$d\omega(E_e) = \frac{2\pi}{\hbar} |T_{if}|^2 \frac{d\phi(E_e)}{dE_e} dE_e, \quad (2.2)$$

where the phase space factor $d\phi$ gives the number of possible final states. The transition matrix

$$T_{if} \propto J_\mu^{\text{hadr}} J^{\mu\text{lept}} \quad (2.3)$$

is proportional to the interaction of leptonic currents J_μ^{lept} and hadronic currents $J_\mu^{\text{hadr}} = V_\mu^{\text{hadr}} + A_\mu^{\text{hadr}}$ with

$$V_\mu^{\text{hadr}} = \langle f | f_1 \gamma_\mu + \frac{i f_2}{m_n} \sigma_{\mu\nu} q^\nu + f_3 q_\mu | i \rangle \quad (2.4)$$

$$A_\mu^{\text{hadr}} = \langle f | g_1 \gamma_\mu \gamma^5 + \frac{i g_2}{2m_n} \sigma_{\mu\nu} \gamma^5 q^\nu + g_3 \gamma^5 q_\mu | i \rangle \quad (2.5)$$

The form factors f_1 , f_2 , f_3 , g_1 , g_2 , and g_3 depend on the squared energy transfer q^2 and account for vector, weak magnetism, induced scalar, axial vector, pseudotensor, and pseudoscalar contributions. f_3 and g_2 are zero due to symmetry arguments. In the limit $q^2 \rightarrow 0$ it is $f_1(q^2 = 0) = g_V$ and $g_1(q^2 = 0) = g_A$, where g_A and g_V are the axial vector and the vector coupling constants from the standard $V - A$ formulation of the weak interaction. g_3 is negligible small.

For neutron β -decay, with $|i\rangle = |n\rangle$ and $|f\rangle = |p\rangle$, the currents read:

$$J_\mu^{\text{lept}} = \langle e^- | \gamma_\mu (1 - \gamma_5) | \nu_e \rangle \quad (2.6)$$

$$J_\mu^{\text{hadr}} = \langle p | g_V \gamma_\mu + \frac{i f_2}{m_n} \sigma_{\mu\nu} q^\nu + g_A \gamma_\mu \gamma^5 + g_3 \gamma^5 q_\mu | n \rangle. \quad (2.7)$$

If we calculate $|T_{if}|^2$ for polarized neutrons and put it into equation 2.2, we get [Jac57]

$$\omega = F(E_e) \left(1 + a \frac{\mathbf{p}_e \mathbf{p}_\nu}{E_e E_\nu} + b \frac{m_e}{E_e} + \langle \sigma_n \rangle \left(A \frac{\mathbf{p}_e}{E_e} + B \frac{\mathbf{p}_\nu}{E_\nu} + D \frac{\mathbf{p}_e \times \mathbf{p}_\nu}{E_e E_\nu} \right) \right) \quad (2.8)$$

for the decay probability. The neutron spin is $\langle \sigma_n \rangle$, \mathbf{p}_e and \mathbf{p}_ν are the momenta of electron and neutrino and E_e , E_ν are their energies. $F(E_e)$ includes the phase-space factor ϕ with corrections and the remaining factors. The β asymmetry A and the neutrino asymmetry B are both parity violating. A triple coefficient $D \neq 0$ would violate time reversal invariance. b is the Fierz interference term. In $V - A$ theory, these correlation coefficients are all functions of $\lambda = \frac{g_A}{g_V}$, the ratio of axial vector and vector coupling constant:

$$\begin{aligned} a &= \frac{1-|\lambda|^2}{1+3|\lambda|^2}, & A &= -2\frac{|\lambda|^2+Re(\lambda)}{1+3|\lambda|^2} \\ B &= 2\frac{|\lambda|^2-Re(\lambda)}{1+3|\lambda|^2} & D &= 2\frac{Im(\lambda)}{1+3|\lambda|^2} \end{aligned} \quad (2.9)$$

In equation 2.9 the asymmetry A is related to λ neglecting f_2 . Small energy dependent influences of proton recoil, weak magnetism and the $g_A g_V$ interferences have to be considered in precision measurements [Wil82]:

$$A(E_e) = A_0 \left(1 + A_{\mu M} \left(A_1 \frac{E_0 + m_e}{m_e} + A_2 \frac{E_e + m_e}{m_e} + A_3 \frac{m_e}{E_e + m_e} \right) \right). \quad (2.10)$$

The uncorrected β asymmetry from equation 2.9 is labeled as A_0 now. $E_0 = m_e + 782keV$ is the maximum energy in neutron decay. The other factors are:

$$\begin{aligned} A_{\mu M} &= \frac{-\lambda+2\kappa+1}{-\lambda(1+\lambda)(1+3\lambda^2)} \frac{m_e}{m_n}, \\ A_1 &= \lambda^2 - \frac{2}{3}\lambda - \frac{1}{3}, \\ A_2 &= \lambda^3 - 3\lambda^2 + \frac{5}{3}\lambda + \frac{1}{3}, \\ A_3 &= 2\lambda^2(1 + \lambda). \end{aligned} \quad (2.11)$$

$A_1 \approx 2.12$, $A_2 \approx -8.66$ and $A_3 \approx -0.87$ are just constants for a fixed value of λ , only $A_{\mu M}$ also depends on the weak magnetism

$$\kappa = \frac{f_2(q^2 = 0)}{f_1(q^2 = 0)}, \quad (2.12)$$

the quantity we want to determine with the first PERKEO III measurement. κ can be related to the anomalous magnetic moments μ_p^a , μ_n^a of proton and neutron via

$$\kappa = \frac{m_n \mu_p^a - \mu_n^a}{m_p} = 1.855,$$

hence we have a theoretical prediction for κ .

2.2. PERKEO III Overview

PERKEO III is a new spectrometer to investigate the decay of free cold polarized neutrons. It was designed to precisely measure asymmetries in the emission direction of the charged decay products. From the asymmetries, detailed information on the weak interaction can be extracted, such as the weak magnetism form factor, described in the section above. In this section we describe the PERKEO measuring principle, and the setup of the first PERKEO III-beamtime to measure this factor at the ILL (Institute Laue-Langevin) in Grenoble, France.

PERKEO measuring principle

The PERKEO measuring principle is quite simple: It makes use of a symmetric setup with two identical detectors. A magnetic field of 150 mT defines two hemispheres for the emission direction of the neutron decay products relative to the neutron spin. The field guides the charged particles to the detectors; in this way a full $2 \times 2\pi$ detection is achieved, without any solid angle corrections to be applied. Figure 2.1 schematically shows the measuring principle of PERKEO III.

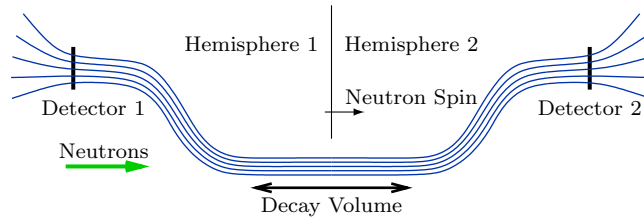


Figure 2.1.: PERKEO III measuring principle: Neutrons are longitudinally polarized; in the decay volume, the spin is aligned with the magnetic field lines represented by the blue lines. In this way, two hemispheres (in and against spin direction) are defined. Picture by Bastian Märkisch.

PERKEO III setup

In the first beamtime we want to determine the weak magnetism coefficient κ in neutron decay from a measurement of the electron asymmetry A . The electron detectors consist each of a large plastic scintillator (Bicron BC400) with mesh photomultiplier tubes (Hamamatsu R5504), suitable to work in magnetic fields, attached on both sides, see figure 2.3.

The experiment is installed at the cold neutron beam position PF1b of the ILL. Figure 2.2 shows a schematic picture of the PERKEO III setup: The neutrons leave the neutron guide H113 and pass the polarizer transmitting only neutrons with the spin in a defined direction, i.e. the beam is fully polarized afterwards. We use a supermirror polarizer and expect a polarization degree of $P \approx 98.5\%$, cf. [Sol02].

To compensate the different detector functions the neutron spin is flipped periodically: A flipping by 180 degrees is equivalent to the interchange of both detectors since the magnetic field direction of the spectrometer is fixed. This is done with a radiofrequency spinflipper successfully used in the last PERKEO II measurements; hence we expect a spin flip efficiency F very close to 100% [Sch04, Mun06].

The purpose of the *shutter-up* is to switch on and off the neutron beam. This way the background in the experimental hall can be measured. The beam is collimated in the beamline to have a defined beam profile and to avoid scattering of neutrons on the instrument walls. To measure the background radiation generated in the beamline, we installed a second shutter, called *shutter-down*. The background from the collimation can now be obtained by subtracting the background with shutter-up closed from the background with shutter-up opened and shutter-down closed.

Behind the shutter-down the neutrons enter the decay volume. Electrons from neutron decay generated here are guided to the detectors by the magnetic field produced by the

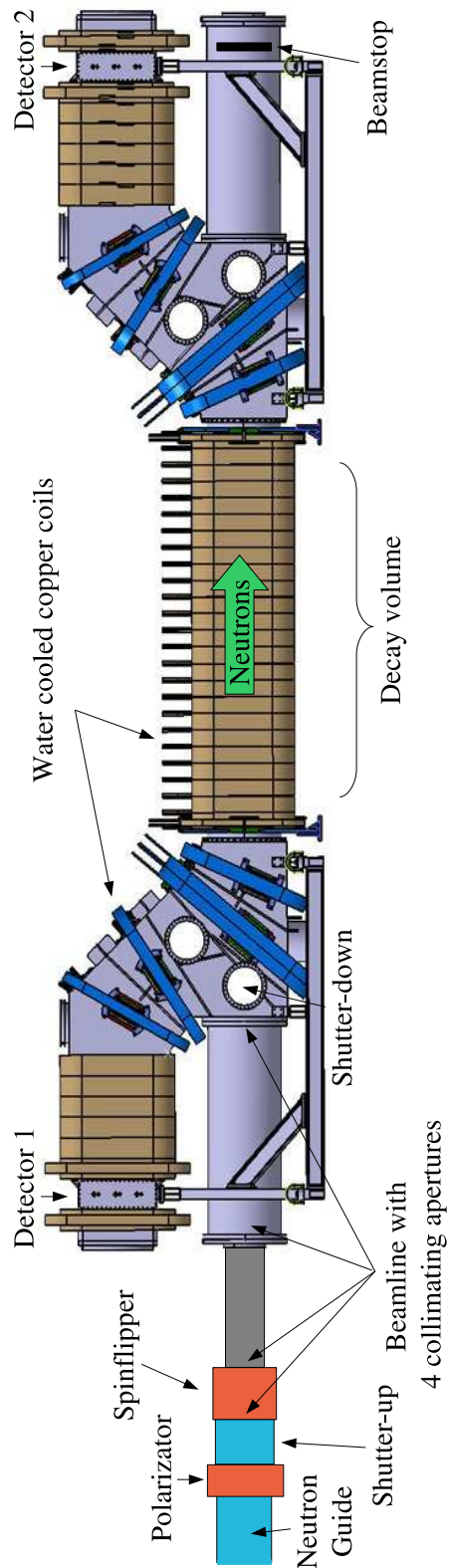


Figure 2.2.: Scheme of the PERKEO III setup to measure the weak magnetism. It is installed at the cold neutron beam position PF1b of the ILL.

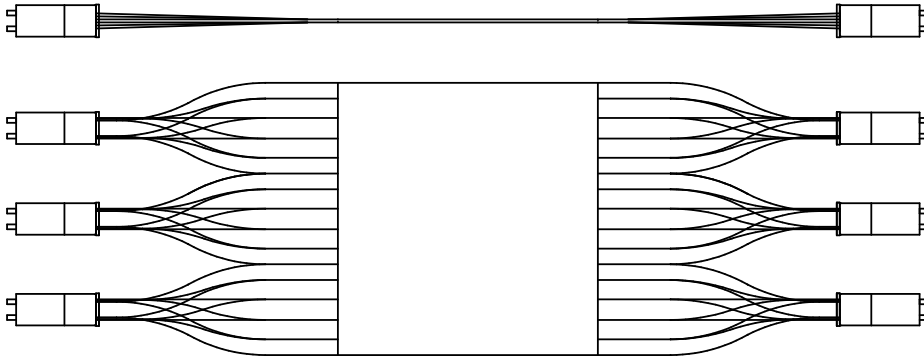


Figure 2.3.: PERKEO III electron detector: The plastic scintillator in the center has an area of $43 \times 45 \text{ cm}^2$ and a thickness of 0.5 cm. The scintillation light is guided to the six photomultiplier tubes via plexiglass lightguides. In the upper part a top view is given. Figure taken from [Mär06].

water-cooled copper coils. Neutrons that did not decay are dumped at the beamstop.

From measured data to weak magnetism

Energy and flight direction relative to the neutron spin are acquired for each detected decay electron. From that the number electrons with energy E_e emitted in $N^\uparrow(E_e)$ and against $N^\downarrow(E_e)$ neutron spin direction are obtained. This yields the experimental asymmetry

$$A_{exp}(E_e) = \frac{N^\uparrow(E_e) - N^\downarrow(E_e)}{N^\uparrow(E_e) + N^\downarrow(E_e)},$$

that is related to the electron asymmetry $A(E_e, \kappa)$, equation (2.10), via

$$A_{exp}(E_e) = \frac{1}{2} A(E_e, \kappa) \frac{v}{c} PF,$$

where v is the electron velocity, P the degree of neutron polarization, and F the spinflipper efficiency. Hence one can determine the weak magnetism coefficient κ from a fit of equation (2.2) to the data.

3. Cooling System

The magnetic field inside PERKEO III is generated by copper coils consisting of 54 segments. It is produced by electrical currents of up to 600 A and consumes a power of 283 kW. Once the field is built up all the electric energy fed to the coils is transformed into thermal energy heating up PERKEO. The heat has to be dissipated to keep the coils from burning out. Therefore we developed a water cooling system pumping 160 l/min through the coils, which are made of copper tubes for this purpose. A heat exchanger connects the cooling circulation supplied at the ILL with the PERKEO's own circulation.

To turn off the power supplies and the pump in case of a failure there are two independent locking mechanisms. First, temperature switches on each single coil segment are connected in series connection. If one of the coils heats up over 70 °C its temperature switch opens the electric circuit and the powersupplies are turned off via an interlock. As a second locking mechanism we developed a water flow watchdog able to detect the flaking of a hose and turn off all critical devices.

The first section of this chapter introduces some theory on fluid mechanics and thermodynamics. This is necessary to understand the calculations to dimension the cooling circulations discussed in section 3.2. The water flow watchdog is presented in section 3.3. The last section shows the results of measurements that approve the correct dimensioning of the cooling system.

3.1. Fluid Mechanics and Thermodynamic Fundamentals

This section gives a short summary of fluid mechanics and thermodynamic fundamentals. This brief introduction derives the formulas needed for the dimensioning of the cooling system. More profound explanations can be found in [Ger77]. The empiric formulars for turbulant flow are given in [Bre03].

Waterflows

The volumetric flux is defined as $\Phi = v \cdot A$ with the velocity of flow v through a surface A .

Loss of pressure due to local constriction

The flux is conserved independent from any local constriction, e.g. from a pipe cross section A_1 to a pipe cross section $A_2 < A_1$:

$$\Phi_1 = \Phi_2 \quad \Leftrightarrow \quad A_1 v_1 = A_2 v_2 \quad \Rightarrow \quad v_2 > v_1$$

Thus, the fluid velocity increases from v_1 to v_2 .

The energy $\Delta W_{kin} = \frac{1}{2}m(v_2^2 - v_1^2) = \frac{1}{2}V\rho(v_2^2 - v_1^2)$ is necessary for this acceleration. It is accomplished by a drop of pressure:

$$W_{p1} = p_1 V = p_1 A_1 v_1 t$$

$$\begin{aligned} W_{p2} &= p_2 V = p_2 A_2 v_2 t \\ \Rightarrow \Delta W_p &= V(p_2 - p_1). \end{aligned}$$

Energy conservation, $\Delta W_{kin} + \Delta W_p = 0$, leads to Bernoulli's Equation:

$$p_1 + \frac{1}{2}\rho v_1^2 = p_2 + \frac{1}{2}\rho v_2^2 = \text{const}$$

From this it follows that every constriction leads to a pressure drop of

$$\Delta p = \frac{1}{2} v_1^2 \rho \left[\left(\frac{A_1}{A_2} \right)^2 - 1 \right].$$

In a closed circulation there is always a return to the initial cross section. So for every constriction there is a dilatation and this effect cancels.

Laminar Flow

For potential flow there is no pressure drop in a tube if the cross section is constant - similar to a perfect conductor, independent of the length. However, potential water flow is completely unphysical since it does not include real world characteristics like turbulence and friction.

Viscosity: For a thin fluid film of thickness x between a solid wall and a movable plate with an area A , the force to move the plate with a constant velocity v in parallel to the wall is

$$F = \eta A \frac{v}{x}.$$

The property of the fluid is described by the viscosity η , which decreases strongly with growing temperatures. For water and many other fluids the viscosity is

$$\eta = \eta_\infty e^{b/T}.$$

For water one gets $\eta_\infty \approx 1.06 \cdot 10^{-6}$ and $b \approx 2000$ by fitting the function above to data from [Nis05], see fig. 3.1.

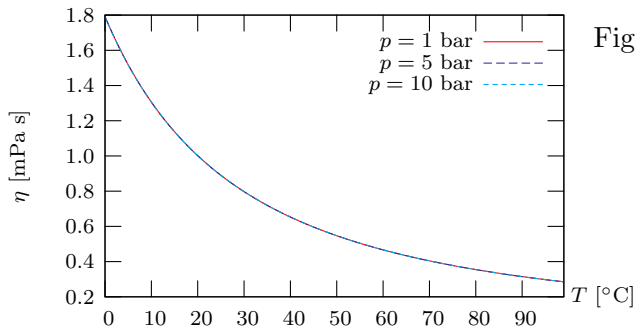


Figure 3.1.: Viscosity of water at different temperatures and pressures. The viscosity is almost completely pressure independent, hence the curves at lower pressures are overlapped by the 10 bar curve.

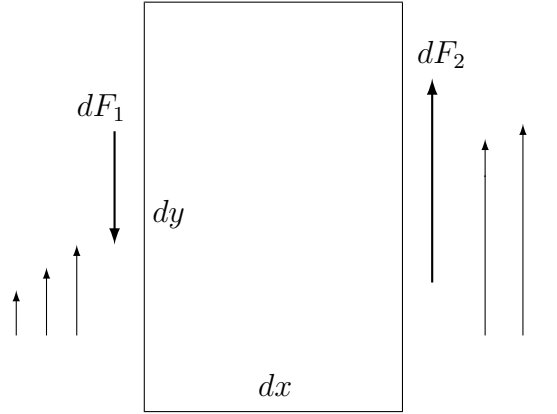


Figure 3.2.: Frictional forces on a small volume of a fluid

Friction forces: Regarding a small volume $dV = dx dy dz$ of a fluid streaming in y -direction and a velocity gradient in x , on the left face (see fig. 3.2) there is a frictional force of

$$dF_1 = -\eta \frac{\partial v}{\partial x}|_{left} dy dz.$$

On the right face in reverse y -direction, there is a force of

$$dF_2 = \eta \frac{\partial v}{\partial x}|_{right} dy dz = \eta \left(\frac{\partial v}{\partial x}|_{left} + \frac{\partial^2 v}{\partial x^2} dx \right) dy dz.$$

Overall on the small volume there acts a force of

$$dF_R = dF_1 + dF_2 = \eta \frac{\partial^2 v}{\partial x^2} dx dy dz.$$

For the general case with velocity gradients in all directions we get

$$\begin{aligned} dF_R &= \eta \left(\frac{\partial^2 v}{\partial x^2} + \frac{\partial^2 v}{\partial y^2} + \frac{\partial^2 v}{\partial z^2} \right) dx dy dz \\ &= \eta \Delta v dV. \end{aligned}$$

Thus the force density is

$$f_R = \frac{dF}{dV} = \eta \Delta v \quad \text{respectively} \quad \vec{f}_R = \eta \Delta \vec{v}$$

for an arbitrary direction of the velocity.

Forces due to pressure: A pressure gradient, e.g. along the x -axis, results in a force on the left face of a small volume (as in fig. 3.3)

$$dF_1 = p dy dz.$$

On the right face, there is also a force

$$dF_2 = - \left(p dy dz + \frac{\partial p}{\partial x} dx dy dz \right).$$

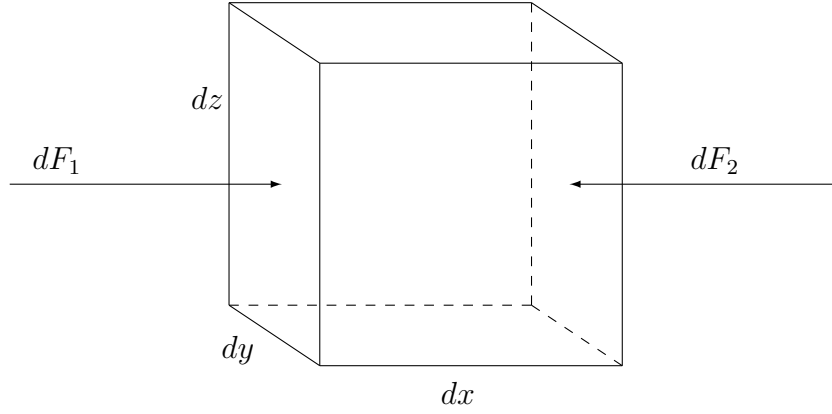


Figure 3.3.: Forces acting on a small volume of fluid caused by pressure

The total force is

$$dF_P = dF_1 + dF_2 = -\frac{\partial p}{\partial x} dV.$$

For arbitrary directions of the pressure gradient we get

$$d\vec{F}_P = -\vec{\nabla} p dV$$

and a force density of

$$\vec{f}_P = \frac{d\vec{F}}{dV} = -\vec{\nabla} p.$$

Laminar flow in a tube: In a tube the fluid is at rest at the boundaries and moves with the highest velocity at the center. On a cylinder of fluid streaming against the y -direction with radius r and length l acts the frictional force

$$F_R = 2\pi r l \eta \frac{dv}{dr}$$

while on its top surface acts the pressure force

$$F_P = \pi r^2 (p_1 - p_2).$$

In equilibrium we have $F_R = F_P$, resulting in:

$$v = v_0 - \frac{p_1 - p_2}{4\eta l} r \quad \text{where} \quad v_0 = \frac{p_1 - p_2}{4\eta l} R^2.$$

R is the radius of the tube.

Through a small hollow cylinder defined by the radii r and $r + dr$ there is the volumetric flow $d\dot{V} = 2\pi r dr v(r)$. For the whole tube we find the Hagen-Poiseuille law (corresponding to Ohm's law in electricity):

$$\dot{V} = \int_0^R 2\pi r v(r) dr = \frac{\pi(p_1 - p_2)}{8\eta l} R^4. \quad (3.1)$$

For a tube with a constant radius R one can write the volumetric flow as $\dot{V} = A \cdot v = \pi R^2 \cdot v$, where v is the mean streaming velocity in the tube. From this together with equation 3.1 we get the pressure drop at mean streaming velocity v :

$$\Delta p = \frac{8}{\pi} \eta \dot{V} \frac{l}{R^4} = 8\eta v \frac{l}{R^2}. \quad (3.2)$$

The *Reynolds Number* is defined as $Re = \frac{v\rho d}{\eta}$, with the density ρ of the medium and the diameter $d = 2R$ of the tube. Now we can write the pressure drop as:

$$\Delta p = 32\eta v \frac{l}{d^2} = \frac{32}{Re} v^2 \rho \frac{l}{d} = \lambda \rho \frac{l}{d} \frac{v^2}{2}. \quad (3.3)$$

We introduced the friction loss factor λ , which is $\lambda = \frac{64}{Re}$ for laminar flows.

Turbulent flow: Turbulent flow or turbulence is a flow with chaotic and stochastic property changes - the opposite of laminar flow. The Reynolds number Re is an indicator whether a flow is laminar or chaotic. Flow in a tube is laminar for $Re < 2000$ and gets turbulent for higher Reynolds numbers (see e.g. [Ger77, Bre03, Stö00]). The critical value of Re also depends on the surface of the tube. One can calculate the pressure drop for turbulent flow just as for laminar flow using equation 3.3, but with different friction loss factor λ . For straight tubes with a plain surface, one can calculate λ with empirical formulas for different ranges of Re (see [Bre03, Stö00]):

$$\lambda = \begin{cases} \frac{64}{Re} & \text{for } Re < 2000 \\ \frac{0.3164}{\sqrt[4]{Re}} & \text{for } 2000 \leq Re \leq 10^5 \end{cases} \quad (3.4)$$

Radiation of heat

Part of the power fed to PERKEO is also dissipated by emission. To estimate the radiated power, we approximate the coils as black bodies. A black body with the surface area A at temperature T emits radiation of the power

$$P = \sigma A T^4, \quad (3.5)$$

where σ is the Stefan-Boltzmann constant $\sigma = 5.67 \cdot 10^{-8} \text{ W m}^{-2} \text{ K}^{-4}$.

Water cooling

To increase the temperature of a water mass m by ΔT , the energy

$$W = c_w \cdot \Delta T \cdot m$$

is necessary. Under standard conditions, the specific heat capacity¹ of water is $c_w = 4183 \text{ J Kg}^{-1} \text{ K}^{-1}$ and the density is $\rho_w = 1 \text{ g ml}^{-1}$. Both can be considered constant here, since their change is only about 2% in the interesting temperature range $T = 10 \dots 70 \text{ }^\circ\text{C}$ and the pressure range $p = 1 \dots 10 \text{ bar}$ - see fig. 3.4.

The other way round, if we want to dissipate the heat produced by the power $P = \frac{d}{dt} W$, we need a water flow of

$$\frac{d}{dt} V = \frac{1}{\rho_w} \frac{d}{dt} m = \frac{1}{\rho_w} \frac{d}{dt} \frac{W}{c_w \Delta T} = \frac{P}{\rho_w c_w \Delta T}. \quad (3.6)$$

¹The specific heat capacity of water at constant pressure is also labeled as c_p .

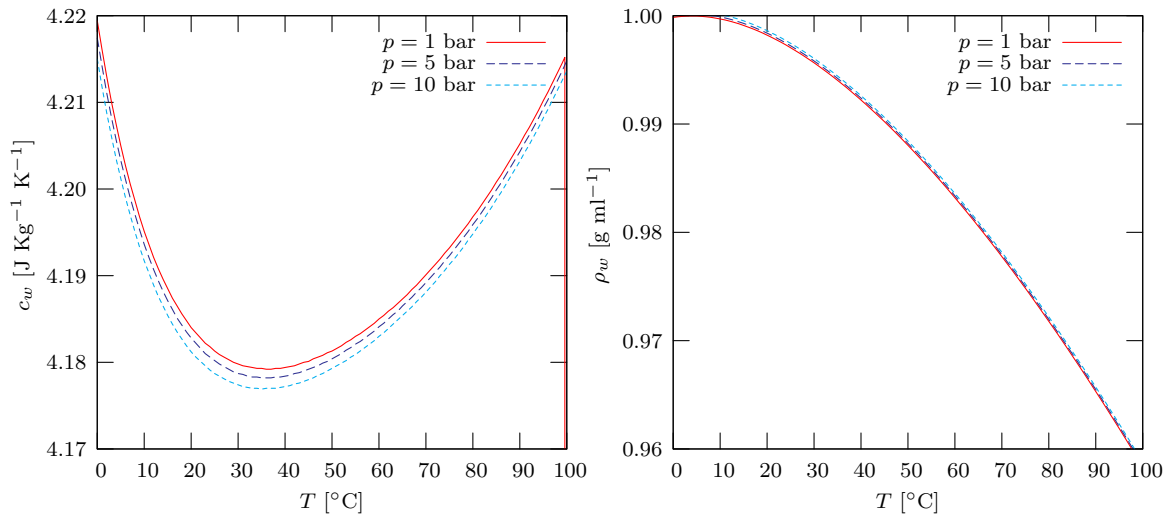


Figure 3.4.: Specific heat capacity (left) and density (right) of water at different temperatures and pressures, ref. [Nis05]. They both change only about 2% in the range of interest ($T = 10\dots70\text{ }^\circ\text{C}$) and can be seen as constant. They can also be considered as pressure independent.

3.2. Cooling Circulations

In this section we give an overview of the PERKEO cooling circulation. It consists of eight subcirculations, see figure 3.5. This division has been chosen on the basis of our calculations, that are discussed in the following. The coil segments are cooled in parallel connection. This is physically more reasonable, since it results in higher flow and less pressure drop.

The properties of the different coil types are shown in table 3.1. The currents and winding numbers given in the table are determined by the material properties and the desired form of the magnetic field. They have been calculated using numerical methods, refer [Mär06]. From the currents and the resistances of the coil segments, one gets the electrical power $P = I \cdot R^2$. We chose an uncritical temperature increase (see row “ ΔT ” in table 3.1) and calculated the necessary water flow (row labeled “Flow”) for each segment using equation 3.6.

The pressure drop in the cooling circulation depends on the lengths and diameters of the coil segments and hoses, as well as on the water flow. We chose a 2 inch firehose for the main circulation and 1 inch rubber hoses for the eight subcirculations. The subcirculations are then split up again and each single coil segment is connected with 8 mm plastic hoses. The hose materials have been chosen on the demands in pressure and temperature resistance. The hollow coil segment themselves have a diameter of 8 mm. We calculated the pressure drop in the segments using equation 3.3, see row “ Δp ” in table 3.1. We also calculated the pressure drop in the 8 mm-in-diameter feed hose (see figures 3.5 and 3.6) for a length of 1 m (in row “ $\Delta p_{8\text{mm}}$ ”) - it is negligible, thus only the pressure drop in the coil segments is relevant.

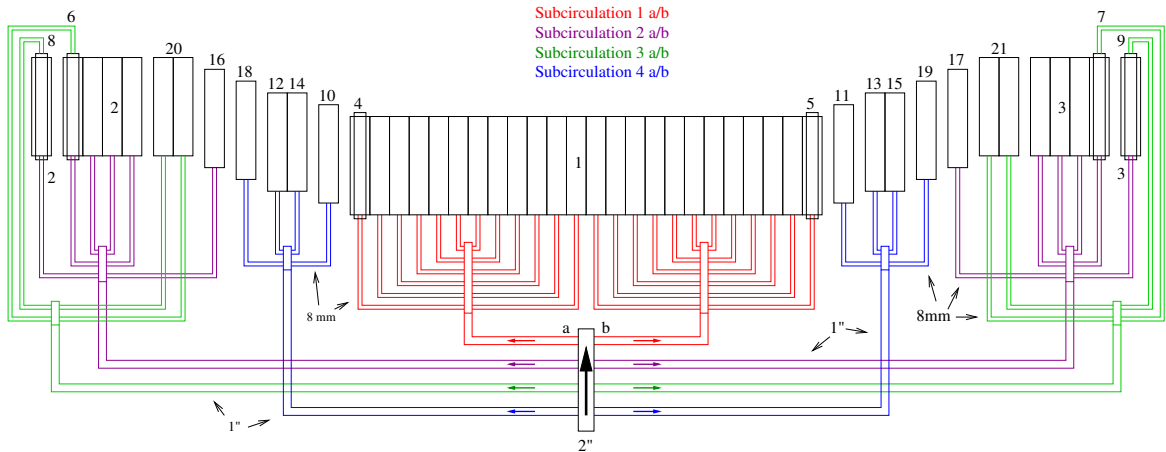


Figure 3.5.: PERKEO III cooling system overview. The coil segments (black) and the hoses with the distributors are shown (colored). All segments are cooled in parallel. For simplicity, only one flow direction is shown (for return direction it looks the same). The coils are labeled with their corresponding number. Adjacent segments belong to the same coil, if not labeled otherwise.

Coils	1	2-3	20-21	4-5	6-9	10-11	12-15	16-17	18-19
Type number	22291	22292	22292	22293	22294	22295	22296	22297	22298
Number of coils	1	2	2	2	4	2	4	2	2
Segments ^a	24	5	2	1	1	1	1	1	1
Windings ^b	8	10	10	3	5	7	6	5	6
Plies ^c	3	3	3	4	6	6	6	4	6
Clear height [m]	0.60	0.85	0.85	0.72	0.95	0.87	0.87	0.87	0.87
Inner width [m]	0.60	0.70	0.70	0.72	0.80	0.77	1.12	0.87	0.87
Length [m] ^d	1525	496	198	38	116	152	155	74	137
Current [A]	570	420	570	570	570	570	570	570	570
Resistance [mΩ]	301	98	39	7	24	32	32	15	28
ΔT [K]	22	22	22	22	29	37	38	25	31
$\rightarrow \dot{V}$ [l/min] ^e	2.66	2.25	4.15	1.58	3.78	3.97	3.97	2.75	4.19
v [m s ⁻¹] ^f	0.88	0.75	1.38	0.52	1.25	1.32	1.32	0.91	1.39
Re	5346	4533	8349	3174	7612	7988	7985	5545	8443
λ	0.04	0.04	0.03	0.04	0.03	0.03	0.03	0.04	0.03
$\rightarrow \Delta p$ [bar]	1.14	1.33	3.88	0.27	3.87	5.50	5.62	1.42	5.48
$\rightarrow \Delta p_{8mm}$ [bar]	0.02	0.00	0.02	0.01	0.03	0.04	0.04	0.02	0.04

^a per coil

^b per ply

^c per coil segment

^d conductor length (sum over all segments)

^e flow per segment

^f mean velocity

Table 3.1.: Different coil types of PERKEO III. The measures and electrical properties of the coils are given in the upper part of the table. In the lower half the calculated flows and the resulting pressure drops are presented.

We merged coil segments with similar pressure drops together to eight subcirculations, labeled 1a/b, 2a/b, 3a/b, 4a/b in table 3.2. Due to the symmetric structure of PERKEO III, always two subcirculations have the same pressure drop. We calculated the pressure drop in the feeding hoses of diameter 1" - it is also negligible.

Name	1	2	3	4
Coils a	1,4 ^a	2,16	6,8,20	10,12,14,18
Coils b	1,5 ^b	3,17	7,9,21	11,13,15,19
Δp [bar]	1.1	1.4	3.9	5.6
Flow [l/min]	31.9	14.0	15.9	16.1
$v_{1''}$ [m/s]	1.05	0.46	0.52	0.53
$Re_{1''}$	20207	8885	10054	10205
$\lambda_{1''}$	$2.65 \cdot 10^{-2}$	$3.26 \cdot 10^{-2}$	$3.16 \cdot 10^{-2}$	$3.15 \cdot 10^{-2}$
$\Delta p_{1''}$ [bar]	0.08	0.07	0.24	0.03

^acoil 4 consists only of one segment and is connected in series with one segment of coil 1

^bcoil 5 consists only of one segment and is connected in series with one segment of coil 1

Table 3.2.: The eight subcirculations of the Cooling System. They are named 1a, 1b, 2a, 2b, 3a, 3b, 4a, 4b. Since subcirculations with the same digit have the same properties, there are only four columns. The second and the third row are important, since they show how the coil segments are merged. Rows four three and four show the corresponding water flows and pressure drops for the subcirculations. The last four rows contain calculated values for the 1" feed hoses of length 20m.

Assembly of the PERKEO III cooling circulation

Figure 3.6 shows the assembly of the PERKEO III cooling circulation schematically. Only one of the eight subcirculations is shown. The pump is connected to the first level distributor (1:8) with an 2" firehose. From there for each subcirculation a 1" hose goes to the second level distributor (1:4 or 1:6), wherefrom a 8 mm hose leads to the separate coil segments. To be able to operate the subcirculations separately, the flow and the return of each subcirculation can be shut via a gate valve. After the gate valve in the flow there is a pressure reducing regulator. In the return, in front of the gate valve, a flow meter is built in. This flow meter is part of the waterflow watchdog described in the next section.

3.3. Waterflow Watchdog

The waterflow watchdog was developed in cooperation with the electronics workshop of the Physics Institute at the University of Heidelberg. It consists of a microcontroller box, a relay box and eight low-cost flowmeters which are part of the PERKEO III cooling circulation.

The microcontroller box is a multipurpose device produced by the electronics workshop featuring a standard USB (universal serial bus) interface and a FPGA (field programmable gate array) by Xilinx as central processing unit. It can carry up to four submodules for various applications. The box is a stand alone device and able to run without any PC. Thanks to the FPGA it can be programmed for a wide range of tasks and new features can be implemented without any change of hardware.

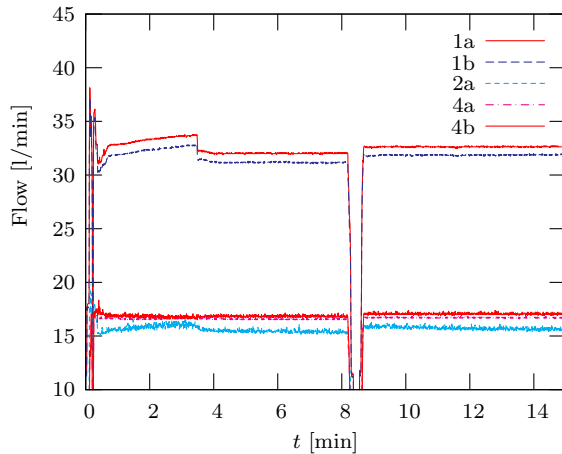


Figure 3.7.: Flows in the subcircuits of the PERKEO III cooling system measured during 15 minutes operation. Not all subcircuits are plotted since their curves would overlap each other. In the first 3.5 min the flow of the pump was calibrated. At $t=8.2$ min we turned the pump off for 0.4 minutes.

Commercial Waterflow Switches

We also tested two commercially available waterflow switches since we expected them to be more reliable and cheaper than a self developed solution. In our tests we monitored the water flow with the flowmeters DFC.9000.100 by Parker to determine the switching point.

The first device tested, the SWP 114 MS from Landefeld has a mechanical functional principle. The water hits onto a plate levering an adjustable magnetic switch. The adjustment of the switching point was very imprecise as a matter of principle. We measured an inaccuracy of more than 30%. The switch flipped between its on and off state in a wide range around the desired switching point, even at a constant water flow.

The second device, SWE 12/24 ES, also from Landefeld, is an electronic device using a calorimetric effect. The sensor is heated up a few degrees above the surrounding fluid. If the medium flows the heat is dissipated which gives a value for the flow rate. An integrated microcontroller compares the flowrate to the desired values and changes the output signal when the rate drops below a certain limit. Again the adjustment of the switching point was quite imprecise. The switching worked good for small flow changes, but was lost for higher changes. We observed a strong hysteresis and a long response time of up to 20 seconds.

In summary, the investigations showed that both commercial flow switches are not sufficient for the purpose of the PERKEO cooling system and made the development of an own solution necessary.

3.4. Measurements

Verification of Calculations

To check if our calculations of the cooling requirements are right and the cooling system is able to dissipate the produced heat we made test measurements. The measurements were made with 5 coil segments (two of type 22295 and three of type 22296) cooled in parallel. The flow was measured with the DFC.9000.100 flowmeter. Table 3.3 shows the result of the tests.

The temperature increase of the coils is much less than calculated. In the calculation we assumed that all electrical power is used to heat the water. In reality only part of the power is dissipated by water ($\approx 68 - 72$ %). We also calculated the power that a black body at the

temperature of the coil emits as radiation ($\approx 5 - 11 \%$), using equation 3.5. The rest of the power is dissipated by convection ($\approx 22 \%$).

Our investigations show that the calculated flows are high enough to dissipate the heat from the copper coils.

Measurement	1	2
I [A]	240	360
U [V]	32	49
P_{el} [W]	7776	17640
\dot{V} [l/min]	15.2	15.2
T_{return} [°C]	21	28
ΔT_m [K]	5	12
ΔT_c [K]	7	17
P_h [kW]	5.3 (68%)	12.7 (72%)
P_e [kW]	0.8 (11%)	0.9 (5%)
P_c [kW]	1.7 (21%)	4.0 (23%)

Table 3.3.: Measurement of the temperature increase of 5 coil segments, electrically series connected, but cooled in parallel. The first part of the table gives the measured electrical parameters and the total water flow. ΔT_m is the measured, ΔT_c is the calculated temperature increase¹. The electrical power was measured with an accuracy of $\pm 4.2\%$, for the temperatures we had an error of ± 1 K and the waterflow was determined with a relative error of $\pm 1.3\%$ In the last part the fractions of dissipated power are shown. P_h is the power used for heating the water, P_e is emitted by a black body at T_{return} and P_c is the remain, dissipated by convection.

¹Provided that all electrical power is used to heat the water.

Data measured with the final PERKEO setup

Table 3.4 shows real world data measured at the ILL. The total pressure drop in the circulation was (7.2 ± 0.1) bar. We calculated the pressure drop in the subcirculations 1a and 1b as to low - it is two times higher than expected. We connected coils 4 and 5 in series each with an other segment of coil 1, this is not taken into account in our calculations. For subcirculation 3a the calculated value is very good, whereas there is a difference of 1 bar between 3a and 3b. This seems to be due to different lengths of the feeding hoses.

It is important to see that equations 3.3 and 3.4 only give estimations. It is an idealization for straight tubes with a plain surface. The estimation for subcirculation 3a fits that well by chance, since we did our estimations for feeding hoses of 20 m length - in reality we have a lengths between 8 m and 16 m. We also completely ignored the pressure drop in the distributors and valves, where turbulences are very likely. And of course we also idealized the coil segments a straight tubes, which in reality have a lot of 90 degree bucklings. We also did not investigate the roughness of the inner surfaces of the hoses and coil segments.

Subcirculation	1a	1b	2a	2b	3a	3b	4a	4b
Flow [l/min]	30.9	30.3	14.5	14.9	15.3	15.8	16.5	16.8
Δp_m [bar]	2.0	2.0	1.5	1.5	3.0	4.0	6.0	6.1
Δp_c [bar]	1.1	1.1	1.4	1.4	3.9	3.9	5.6	5.6

Table 3.4.: Real data measured during operation of Perkeo III at the ILL. Shown are the flows in several subcircuits, the measured pressure drop Δp_m and the calculated pressure drop Δp_c . The measuring error for all pressures is ± 0.1 bar, for the flows it is ± 0.1 l/min. Almost all pressure drops have been calculated as too low. The calculated value for subcirculation 3a fits by chance (see text for an explanation).

Summary

This is the first water cooling system ever used for a PERKEO experiment. In this first attempt, the cooling works well and the calculations gives an order of magnitude agreement. Comparison of calculated and measured values shows that the pressure drop in the distributors is not negligible.

4. Data Acquisition

In the Perkeo III experiment data acquisition consists of transformation of the scintillation light to electric pulses, conversion to digital values and transport of the data to the measuring PC, where it is stored permanently. To control the spinflipper and calibration measurements are also tasks of data acquisition system.

In this chapter we first give an overview of the components used. Then we present the acceleration of the data read out and introduce the new software *Dackel*. We also show our investigations of the ADC linearity and the results of an alternative photomultiplier test.

4.1. Overview

The Aim was to reuse and improve the already available hardware of the Perkeo II experiment to handle the requirements of Perkeo III. In this section an overview of the used electronic components is given including a short description of every device. Figure 4.1 shows the setup used in the experiment.

Personal Computer

For this experiment data acquisition is done with a standard PC with a 1666 MHz CPU and 256 MB RAM. To reduce the risk of data loss, two new identical 300 GB harddisks were installed as a level 1 software raid. As a backup system we have second a PC with exactly the same configuration. Communication with the VME¹ devices is done with the SIS 1100/3100 PCI² to VME link by Struck Innovative Systems. It consists of the SIS3100 PCI card on PC side and the SIS 1100 card on VME side.

Different Linux distributions together with different versions of the driver for the SIS device have been compared for performance and stability. At the time of the tests, the only driver for Linux 2.6.x was the unofficial version 2.02. Due to inconsistencies in the Linux Kernel API in the 2.6.x series, some additional adjustments on the driver had to be done. The different Linux versions all showed the same performance and high stability. For the final setup we chose OpenSuSE Linux 10.1, since the latest driver version 2.04 for the SIS 3100 was tested on this Linux distribution by the Struck.

VME Devices

We use a SIS 3000 VME crate (also by Struck) for our VME components described below.

Analog to Digital Converter: An analog to digital converter (ADC) is an electronic device that converts continuous analog signals to discrete digital numbers. The properties characterizing an ADC are introduced in section 4.4.

¹Versa Module Eurocard bus. A bus standard widely used for data acquisition in physics.

²Peripheral Component Interconnect. The Bus system of today's standard PCs.

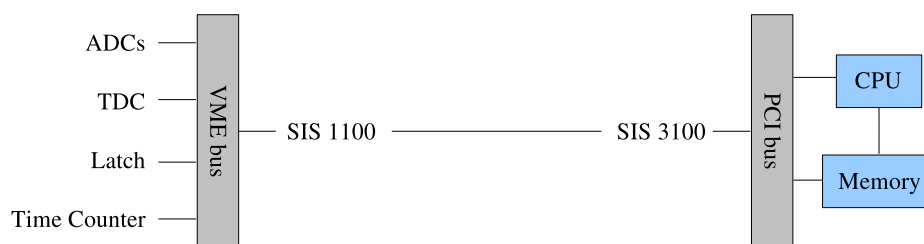


Figure 4.2.: The link between VME and PCI bus. Only the most important components are shown.

We use four DL642A three-channel gated integrators to measure the energy spectrum of the electrons from neutron decay. A capacity on each of its inputs is used to integrate over the photomultiplier pulses. Since this way a charge Q is converted to a digital value, one also calls such devices $QADC$ or QDC . The DL642A was developed at the electronic workshop of the Physics Institute, University of Heidelberg. Internally the DL642A is built using 14-bit ADC chips, type AD7484 by Analog Devices.

Time to Digital Converter: A time to digital converter (TDC) is a device for converting input pulses into a digital representation of their time indices. A TDC outputs the time of arrival for each incoming pulse. The V767A 64 channel multihit TDC by CAEN is used for Perkeo III to recognize the backscattering of electrons on the scintillators.

Latch: In digital circuits, a latch is just a particular usage of the simple flip-flop. More general, a latch is an electronic module that stores a digital value given on its input. We have a SIS3600 32-bit VME Multi Event Latch by Struck to store several information of each event, such as spin flipper status, shutter status or which detector triggered first.

Time Counter: The time counter DL643A1 from the electronics workshop of the Physics Institute is a device that saves the arrival times of incoming trigger as absolute values. This is realized with an internal 1 MHz clock and a 24-bit wide FIFO to store the values. One can see the time counter as a simple TDC. It is used to obtain a unique arrival time for each incoming event during a measuring cycle. This way, correlations in the data caused by systematic effects can be detected.

Digital IO: The Digital IO DL646F is another device built by the electronics workshop. It has three outputs and one input. It is used for various purposes, e.g. to control the spin flipper.

StartStop Module: The StartStop Module is a device (developed at the ILL) generating a signal that is used to enable and disable other devices. The busy signals from the TDC, the Latch and the ADCs are fed into the StartStop Module. This way it is possible to have the devices enabled for an exact time, with automatic compensation of the dead time.

Counters: The DL636G counters are devices that increase the value of their internal registers when triggered. We use several counter for various purposes, such as totaling the number of events or determination of the dead time.

Other Devices:

In addition to the VME devices we use many other NIM³ and one CAMAC⁴ module. Most of them are fan-outs (digital and analog ones) or simple logic elements, such as digital AND, OR and NOT. Also some gate generators are used. Discriminator and the coincidence unit are both described below.

Constant Fraction Discriminator: A constant fraction discriminator is a signal processing device used to detect pulses (e.g. from scintillation detectors) with a certain pulse width and a characteristic rising time. It is often used, if the rising time is higher than the desired time resolution. In this case it is impossible to use a simple threshold triggering, cf. figure 4.3.

We use the C808 16 Channel Constant Fraction Discriminator by CAEN for the CAMAC bus to detect the electron signals from our photomultipliers.

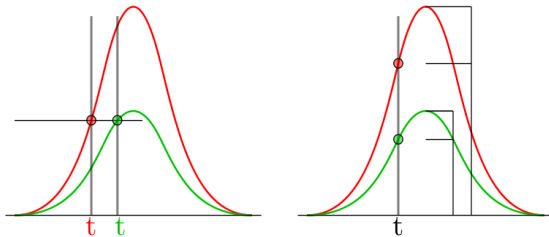


Figure 4.3.: Comparison of two triggering methods. The trigger time is dependent on the pulse height if simple threshold triggering is used (left). A constant fraction discriminator avoids this by triggering when a certain fraction of the total pulse height is reached (right). Picture taken from [Wik06].

Coincidence Unit: A NIM-coincidence unit is used to avoid random pulses from single photomultipliers to be detected as an electron signal. It has several inputs and one output. The output only gives a signal if there is a signal on at least two inputs at the same time what suppresses random pulses efficiently.

4.2. Data Rate Improvement

For the last Perkeo II experiments (2003, 2004), data acquisition was changed from CAMAC to VME, which brought a serious improvement of the deadtime, ref. [Sch04]. The maximum data rate in these experiments was 600 Hz, including background signals. Eight ADC values were stored resulting in 21 bytes of information per event [Mun06], resulting in a data rate of 0.01 MB /s. For Perkeo III we expect a decay rate of approx 30 kHz. The number of bytes per event is 40 bytes since 12 ADCs values have to be stored, so the data acquisition system has to process at least 1.1 MB / s. One part of this thesis is the improvement of the existing VME hardware to cope with the data rate increase by two magnitudes. This was

³Nuclear Instrumentation Module, a standard for electronic devices used in experimental particle and nuclear physics.

⁴Computer Automated Measurement And Control - a standard bus for data acquisition and control used in nuclear and particle physics and in industry.

achieved by using the single word DMA⁵ routines of the SIS3100/1100 PCI-to-VME link and implementing new features to the existing VME devices.

In this section we first give a short introduction into the different hardware access methods of PCs. Then we describe the SIS DMA mode and the hardware upgrades mentioned above. Finally we present the new data rates possible with the Perkeo data acquisition system.

PC Hardware access modes

In modern PCs there are several methods to transfer data between the internal devices such as programmed input/output (PIO), interrupt driven communication and direct memory access (DMA). Here only a very brief introduction to PIO and DMA is given, necessary to understand how the acceleration of the data transfer was possible. More detailed information on this topic can be found in the literature, e.g. [Rub02, Sta01].

PIO: In programmed input/output mode, all data transferred between a device and the memory has to go through the CPU. For reading a certain amount of data words from a hardware device to the computer's memory the CPU has to request each single word from the hardware. Then it has to wait until data is delivered and write it to the memory. To writing data to a device, the same has to be done the other way round. The CPU thus is occupied during the data transaction and can't do other things in the mean time.

DMA: Devices capable of direct memory access can write data directly to the computer's memory without going the way via the CPU. The CPU only has to tell the hardware to start a data transfer and then is notified when the transfer is finished. In the mean time the CPU can do other things, which improves performance a lot.

Today's PCs use the PCI bus for communication between its internal components. Besides the more economical consumption of CPU power using the DMA mode of PCI devices has another big advantage: Every data transfer over the PCI bus has a certain overhead taking some time. This overhead is due to the bus protocol, containing e.g. bus arbitration, addressing, etc. In PIO mode this overhead is done for every transferred word, while in DMA mode this is done only once for a block of many data words.

VME access modes

The VMEbus architecture provides a variety of address spaces and data widths. Data transfer cycles can be either single cycle or block transfer.

Single cycle mode: In single cycle mode the bus protocol (e.g. addressing) is done for every single data word transferred. This mode can be compared to the PIO in PC data transfer (see above).

Block transfer mode In block transfer a block of data words is transferred at once, which avoids unnecessary overhead. This mode is similar to the DMA mode of the PC.

⁵Direct memory access.

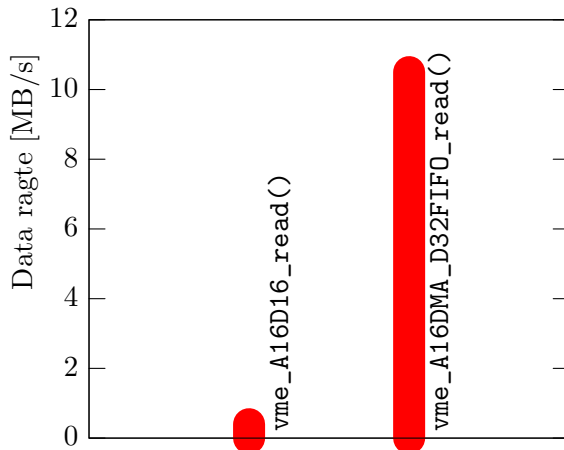


Figure 4.4.: Date rate comparison for the different read out modes. The average date rate for the PIO access is 0.4 MB/s, shown on the left. On the right is the average data rate of 10.5 MB/s for the DMA access.

Upgrades of the VME Modules

The ADCs, the timer counter and the normal counters (all manufactured by the electronic workshop) only supported the VME single cycle mode with 16-bit addressing and 16-bit data words. In this mode we only got a data rate of 0.48 MB/s, cf. Figure 4.4.

By using the “*Single word DMA routines*”, a special feature of the SIS 3100/1100, we get a more than 20 times higher data rate of 10.5 MB/s (see right bar in figure 4.4. The routines do DMA transfers on PCI bus, while on the VME bus the data is transferred in single word mode. They yield a substantial gain in performance since the PCI overhead is reduced and the VME bus is fast enough even in single word mode. The fast DMA routines do only work with data sizes of 32-bit, since this is the width of the PCI bus. Therefore all critical components have been upgraded by the electronic workshop, and now are accessible in 32-bit data mode. Due to technical reasons it was not possible to enable also 32-bit addressing. The driver of the SIS 3100 does not supply a single word DMA routine for 16 Bit adress mode, which was then implemented by us.

For the data rate determination of the DMA accesses we developed some macros that allow time measurements independent of timer interrupts. Since they can be reused for further improvements of the hardware or in general for time measurements, they are presentet in appendix A.

Data rate in the experiment

The data rates have been improved by one magnitude and are now about 10 MB/s. In the final setup there have to be read twelve ADC values, four TDC values, one TimerCounter value and one Latch value per event. For each of these values a 32-bit access has to be done. The result is a data rate of approximately 2 MB/s for a decay rate of 30 kHz. This calculation shows that the hardware readout is fast enough to cope with the expected data rates.

In addition we tested the complete electronics setup with a periodic signal from afunction generator model 162 by Wavetek as trigger. In our tests the electronics worked perfect up to a frequency of $f = 80$ kHz. However this test is far from reality, where we trigger on electrons from neutron decay. The decay is a random process, with the expected *mean* rate of 30 kHz. So several events will have a time distance of significantly lower than $T = \frac{1}{30}$ ms.

To test the electronic in a more realistic way, we programmed the function generator to give random pulses. The electronics could easily handle signals with that rate with a mean

frequency of up 50 kHz.

4.3. Dackel

Dackel is an acronym for “Data Acquisition and Control of Electronics”. The “k” in Dackel is just a placeholder and makes the acronym easily remindable, because Dackel is also the German word for Teckel or Sausage Dog. Dackel is the successor of VME MOPS and the old MOPS which are the “Measuring and Operating Systems” of PERKEO and PERKEO II. Mops is the German word for Pug, which is also a dog race, so Dackel suits well as name for the new data acquisition system.

Since we have use the single word DMA routines described in section 4.2, it was easier to write a new data acquisition software from scratch than try to reuse the old one. Additionally, because of the higher data rates, the use of compression is of advantage which is easier to realize when writing new code. Dackel was written in standard C++ with the GNU compiler and thus compiles on every common Linux system with installed drivers for SIS 3100.

The job of Dackel is to initialize the VME hardware, control the measurement, read the measured data from the devices, and write it in a compressed binary format to the harddisk of the PC. Controlling the measurement means to program the StartStop card to do deadtime compensation, start and stop the acquisition, check consistency of data and to drive the spin flipper.

In former PERKEO experiments the data aquisition program (MOPS) also controlled the shutters as well as the scanner used for calibration. Now this is done with NOMAD [Nom06], a control software of the ILL instrument control group. We enabled both software packages to work together.

In this section the measuring scheme, the data format and its usage of Dackel are documented.

Measuring scheme

In a measurement, data is taken with different configurations of the instrument which are determined by the states of the beam, the shutters, and the calibration scanner. For each of this configurations a single data file is created. Internally, a file is structured in so called cycles that contain the data of a certain measuring time. The duration of a cycle is adjustable, a typical value is ten seconds.

The weak magnetism form factor is calculated from the electron asymmetry in neutron β decay. To cancel out differences between the two detectors, the spin is flipped in the measurements (see chapter 2.2). Since part of the count rate on the detectors is always caused by background radiation, linear drifts of the background would significantly distort the asymmetry measurement. To avoid this, we use a spin flipping scheme as shown in figure 4.5 which was already used in all former PERKEO experiments (see e.g. [Mun06]). Since Dackel drives the spin flipper, it also has to take care of the spin flipping scheme. For each spin flipper state (can be *on* or *off*), a new cycle is started. Example:

- The spin flipper is set to *on*.
- Wait until all neutrons that were in the beam before the flipper was changed have passed the decay volume (which is typically some μs).
- Start measuring one cycle (typically 10 seconds).

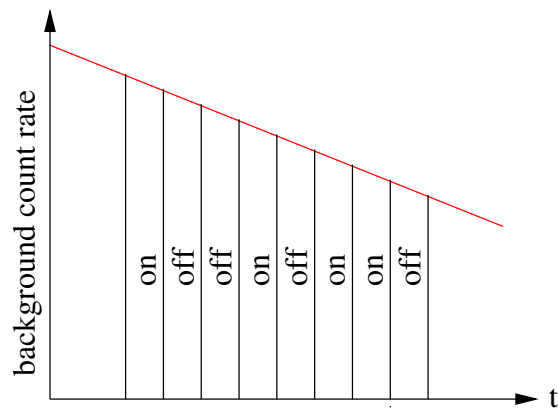


Figure 4.5.: Measuring scheme for the spin flipper of Perkeo III. The area below the line with *on* and *off* states is equal. This way a linear drift in the count rate cancels out.

- Stop measuring
- Set spinflipper to the next state.

Usage

All options of Dackel can be set via command line parameters to enable easy instrument control using Linux shell scripts. To get the available parameters the program has to be invoked in the following way:

```
./dackel -h
```

Figure 4.6 shows the output of this invocation. Most of the options are self-explaining, such as the setting of the VME hardware addresses. One can also set some TDC parameters explained in [Cae01]. The time to measure is the length of one cycle, it is set via parameter `-t <time>` and its unit via `-u <unit>`. Dackel periodically reads out the buffers of the VME devices. For low data rates a sleep time between the read outs can be set with `-s <time>`. So an unnecessary polling on empty buffers can be avoided. The compression level of the zlib routines (see [zlib]) can be set between 0 and 9 with the parameter `-z <level>`. If the data acquisition system can't handle the incoming data rate, it is a good idea to decrease the compression level. Data is written in the format described below to the output file specified with `-o <file>`. The pattern of the spin flipping scheme can be changed via `-S <scheme>`, where `<scheme>` is a string of 0 and 1. The scheme shown in fig. 4.5 is "10010110" for example. Dackel waits the time given by `-p <time>` between the spinflips and loops over the scheme a number of times given by `-l <number>`.

Since most of the options do not change after the data acquisition is set up, the options can also be written in a configuration file which is read by Dackel at startup. The configuration file is specified via the parameter `-f <file>`. If no configuration file name is given, the default behavior is searched in the current directory in a file named `dackel.cfg`.

Data Format

For each event 12 ADC values (each 16-bit), 2 TDC values (each 32-bit), one time counter value (32-bit), and one latch value (32-bit) have to be stored. This results in 40 bytes of data per event, corresponding to a data rate of 1.2 MB/s for the expected decay rate of 30 kHz. To reduce the necessary disk space to store the data Dackel uses a binary file format which in

```

-----
dackel
-----

usage: ./dackel [options]

options:
-h,          --help          shows this help
-T,          --test          only show settings and exit
-f <file>,   --config-file <file> use <file> as config file

ADC settings:
-A <addr>,   --adc0-addr <addr>   set address of adc0 (in hex)
-B <addr>,   --adc1-addr <addr>   set address of adc1 (in hex)
-C <addr>,   --adc2-addr <addr>   set address of adc2 (in hex)
-D <addr>,   --adc3-addr <addr>   set address of adc3 (in hex)

TDC settings:
-T <addr>,   --tdc-addr <addr>   set tdc address (in hex)
-E <ch#>,    --tdc-channel1 <ch#> set tdc channel 1
-F <ch#>,    --tdc-channel2 <ch#> set tdc channel 2
-G <tics>,    --tdc-window-width <tics> set tdc window width (clock tics)
-H <tics>,    --tdc-window-offset <tics> set tdc offset (clock tics)

other settings:
-U <addr>,   --tc-addr <addr>     set tc address (in hex format)
-L <addr>,   --latch-addr <addr>  set latch address (in hex format)
-I <addr>,   --io-addr <addr>     set io module address (in hex)
-J <addr>,   --cnt1-addr <addr>   set counter1 address (in hex)
-K <addr>,   --cnt2-addr <addr>   set counter2 address (in hex)
-M <addr>,   --startstop-addr <addr> set startstop address (in hex)
-d <path>,   --sis1100-device <path> set sis1100 device file to <path>
-t <time>,   --measure-time <time> set measure time
-u <unit>,   --measure-time-unit <unit> set unit for measuretime, can be:
                                     100ns,1us,10us,100us,1ms,10ms,100ms
-s <time>,   --sleep-time <time>  set sleep time (in us)
-z <level>,  --gz-level <level>         set gz compression level
-o <file>,   --data-file <file>   set output file
-l <file>,   --log-file <file>    set log file
-S <schema>, --spin-flip-schema <schema> set spin flip schema
-r <loops>,  --spin-flip-loops <loops> set number of spin flip loops
-p <time>,   --spin-flip-pause <time> pause between spinflips (in us)

all numbers must be given in decimal format, if not explicitly specified

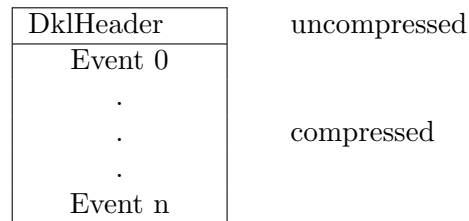
```

Figure 4.6.: Commandline parameters of Dackel. For every option, there is a short parameter (first column) and a long parameter (second column). Some parameters require an argument indicated by `<argument>`.

addition is compressed with the zlib⁶ routines. The file consists of an uncompressed header (this is because of performance and easier programming) followed by the data for each event, see figure 4.7.

The contents of the header is shown in table 4.1. The “*Magic Byte*” is just a marker indicating the `dk1`-file format. *Header length* is the total length of the header in bytes. The date structure is explained in table 4.2. *Total event count* is the total number of events in the file. *Modus* is a 16 bit pattern containing setup information of the measurement, see right part of table 4.1. The field `sfs_length` is the length of the spin flipping scheme (which is eight in the scheme mentioned above). `sf_loops` is the number of spin flips loops. *First cycle ID* is the unique identification number of the first cycle in the file. *File OK* is 1 if the measurement ended the usual way and 0 if there was an interruption. At the end of the header an arbitrary number of counters can be saved. Per counter there is one countervalue for each cycle.

Figure 4.7.: The file format of Dackel. The uncompressed size of a single event is 40 Bytes.



Offset	Description	Bytes
+0x0	Magic Byte	1
+0x1	Version	1
+0x2	Header length	4
+0x6	Date (see <code>dk1_date</code>)	8
+0xe	Total event count	4
+0x12	Modus	2
+0x14	Comment	256
+0x114	<code>sfs_length</code>	1
+0x115	<code>sf_loops</code>	1
+0x116	First cycle ID	4
+0x11a	Number of cycles	4
+0x11e	File OK	1
+0x11f	Number of counters	1
+0x120	Counter data	x

Bit	Meaning
10	Test
9	Scan
8	Source 5
7	Source 4
6	Source 3
5	Source 2
4	Source 1
3	Shutter-Down
2	Shutter-Up
1	Main Shutter
0	Beam

Table 4.1.: Header structure of the `.dk1`-files on the left. On the right the contents of the `modus` field is shown.

The Event data is stored in a C-structure shown in listing 4.1. This structure is directly written to the outputfile via the zlib routines. To extract the compressed data to ASCII format the tool `dk12dat` has been written. The measured data can be imported in ROOT⁷ with the tool `dk12root`. For more detailed information refer to the source code [Dackel].

⁶zlib, a general purpose compression library, see [zlib] for more information.

⁷An object-oriented data analysis framework developed at CERN, see [Root].

```
typedef struct {
    u_int16_t adc00,adc01,adc02; // adc0
    u_int16_t adc10,adc11,adc12; // adc1
    u_int16_t adc20,adc21,adc22; // adc2
    u_int16_t adc30,adc31,adc32; // adc3
    u_int32_t tdc1,tdc2;
    u_int32_t tc;
    u_int32_t latch;
} EventStruct;
```

Listing 4.1: Structure of the data for one single event in C programming language.

Offset	Description	Type	Bytes
+0x00	year (ad)	u_int16_t	2
+0x02	month (1=Jan, 12=Dec)	u_int8_t	1
+0x03	day (1-31)	u_int8_t	1
+0x04	hour (0-23)	u_int8_t	1
+0x05	minute (0-59)	u_int8_t	1
+0x06	second (0-59)	u_int8_t	1
+0x08	dummy	u_int8_t	1

Table 4.2.: The date structure of the Dackel file format.

4.4. Linearity of ADCs

Although the ADCs DL642A have already been used in former measurements, they showed a strange behavior when we tested them by measuring a Bi-207 spectrum, see figure 4.8. By merging data from neighboring channels of the ADCs (also called "*binning*"), one gets a better result. This solves the problem, but one can not use the full resolution of the ADC this way. This was the cause to further investigate the ADCs.

ADC characteristics

An ADC can be characterized on this properties:

- The dynamic range D of input voltages.
- The resolution k , given as the number of bits used to encode the output numbers i . One also speaks of channel numbers or channels instead of output number. It follows $0 \leq i \leq 2^k - 1$.
- The sampling frequency $\frac{1}{\Delta t}$. Analog input signals are also continuous in time whereas the output values refer to a discrete point in time.

A range $\Delta U(i)$ of analog input values is mapped to each digital output value i , thus

$$D = \sum_{i=0}^{2^k-1} \Delta U(j).$$

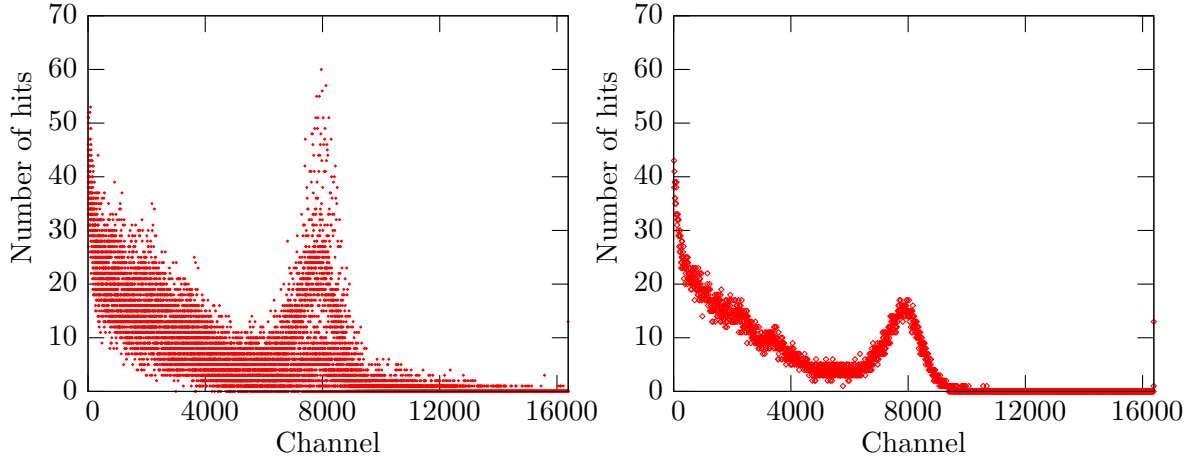


Figure 4.8.: Bi-207 spectrum measured with one of the ADCs before improvement of non-linearity.

ΔU is also called channel width. A perfect ADC would have a constant width for all channels. In reality all ADCs suffer from non-linearity, due to physical imperfections. That means that their output deviates from a linear function of their input. Their non-linearity is quantified by the *differential non-linearity*

$$\text{DNL}(i) = \frac{\Delta U(i) - \overline{\Delta U}}{\overline{\Delta U}}, \quad (4.1)$$

that measures the non-constancy in width of each channel. It is of special importance for spectrum measurements, ref. [Leo94]. The *integral non-linearity*

$$\text{INL}(i) = \sum_{0 \leq j \leq i} \text{DNL}(j), \quad (4.2)$$

is the deviation from the linear correspondence between height of the analog input signal and the channel number.

The integral and differential linearities are related quantities by definition, cf. equation 4.2. Because the differential non-linearity for different channels can be of different sign, it is possible that an ADC has good integral linearity, but a poor differential linearity. Therefore the differential non-linearity is the more crucial of the two parameters. Binning cancels out the effect of a periodic DNL, but has the disadvantage that resolution is lost.

Histogram Method to Determine the Non-Linearity

The non-linearity of an ADC can be determined with the so called histogram method, ref. [Lab]. A ramp signal covering the full dynamic range of the ADC is given as an input signal. After a large number of periods a histogram is built from the measured data. Every channel i of the ADC should have been hit approximately the same number of times $N(i) \approx \overline{N}$, where \overline{N} is the mean number of hits per channel. It is easy to see that the relative channel width is equal to the relative number of hits for each channel:

$$\frac{\Delta U(i)}{\overline{\Delta U}} = \frac{N(i)}{\overline{N}}$$

The differential non-linearity then is

$$\text{DNL}(i) = \frac{N(i)}{N} - 1$$

Measurements

We investigated the linearity of our ADCs by applying the histogram method described above. We used a rampsignal with Amplitude $U = 2.62\text{V}$ and frequency $f_1 = 1\text{ Hz}$. The data was sampled with a frequency of $f_2 = 25\text{ kHz}$. Figure 4.9 (left plot) shows the differential non-linearity of one of our ADCs before its update done by the electronic workshop. It has a strange structure for some channels which leads to the bad spectrum in figure 4.8. By shielding we got rid of the effect. The shielding consists of a copper plate connected to ground that was glued on the body of IC⁸ that implements the ADC. All of our ADCs showed a similar behavior and were thus upgraded.

After the upgrade, the differential non-linearity improved a lot, what can be seen in the right plot in fig. 4.9. In figure 4.10 the integral non-linearity before and after the upgrade are shown. Before there was a periodic structure in the integral non-linearity corresponding to the large DNL above channel 600, that vanished due to the update.

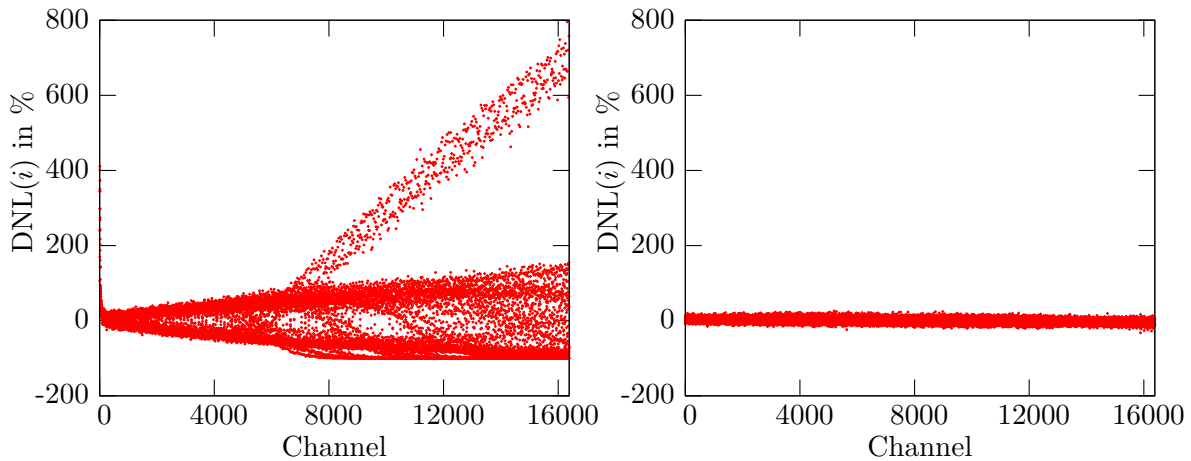


Figure 4.9.: DNL before improvement (left) and afterwards (right).

⁸integrated circuit

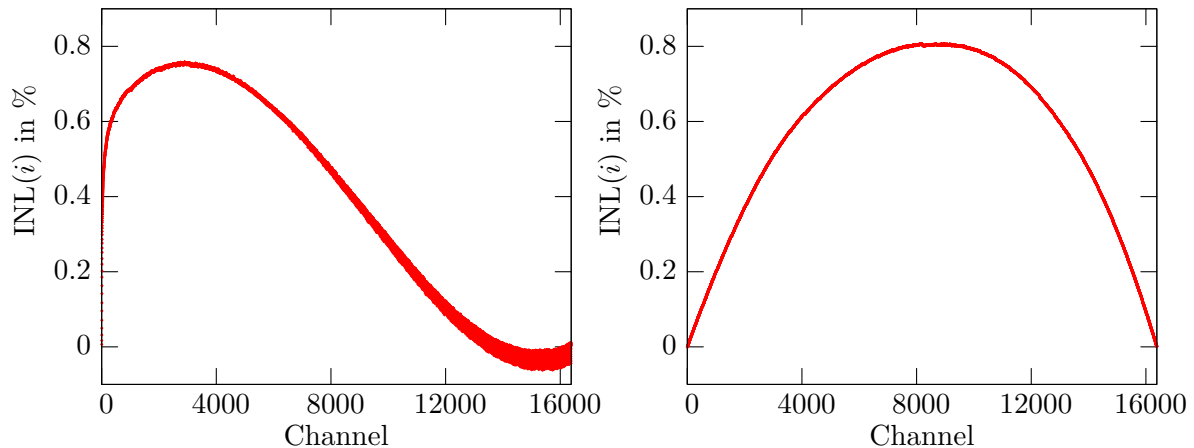


Figure 4.10.: INL before improvement (left) and afterwards (right). The integral non-linearity is below 1% in both cases. This OK for our measurements since the dectector calibration is limited by other factors.

4.5. Photomultiplier Tests

The electron detector of PERKEO III consists of a large plastic scintillator (Bicron BC400) with photomultipliers (PMT for short) readout attached on two sides (see figure 2.3). For PERKEO III we use twelve already existing mesh photomultipliers R5504 from HAMAMATSU. These work reliable in very high magnetic fields of at least 0.5 T and already proved their worth in former PERKEO experiments [Rei99, Kre04, Mun06], but are limited in quantum efficiency. Since the PMT only needs to work in a 20 mT magnetic field in this experiment, we searched for less expensive standard PMTs with higher quantum efficiency as alternatives.

For this purpose the PMT 9214SB from Electron Tubes was tested, is equipped with a built in mu-metal shield and a second external shield for operation in electromagnetic fields. The scintillator BC400 has a maximum of emission at a wavelength of $\lambda = 423$ nm, cf. [BC400]. At this wavelength the quantum efficiency of the PMT 9214SB is about 27%, see [PMT9214SB].

Setup

A 5×5 cm² piece of a 5 mm thick BC404 plastic scintillator was fixed to the PMT using high vacuum grease. As an electron source we attached a Bi-207 conversion source directly behind the scintillator. The Bi-spectrum has a high β -peak at 997.9 keV. The rest of the spectrum cannot be resolved due to bad energy resolution in this setup and additional gamma-background of the source, see figure 4.11. The tests were done at normal pressure of about 1 bar. To generate the magnetic field we used water cooled Helmholtz coils.

Drift Test without magnetic field

The drift test was done without any additional magnetic shield, so the PMT was exposed only to the magnetic field of the earth. We performed measurements for 15 minutes repeated for several hours. After an usual start-up drift within the first 2 hours, the following 19 hours

the gain stayed constant below the 1% level, cf. figure 4.11. The test was continued for 48 hours, without any significant change.

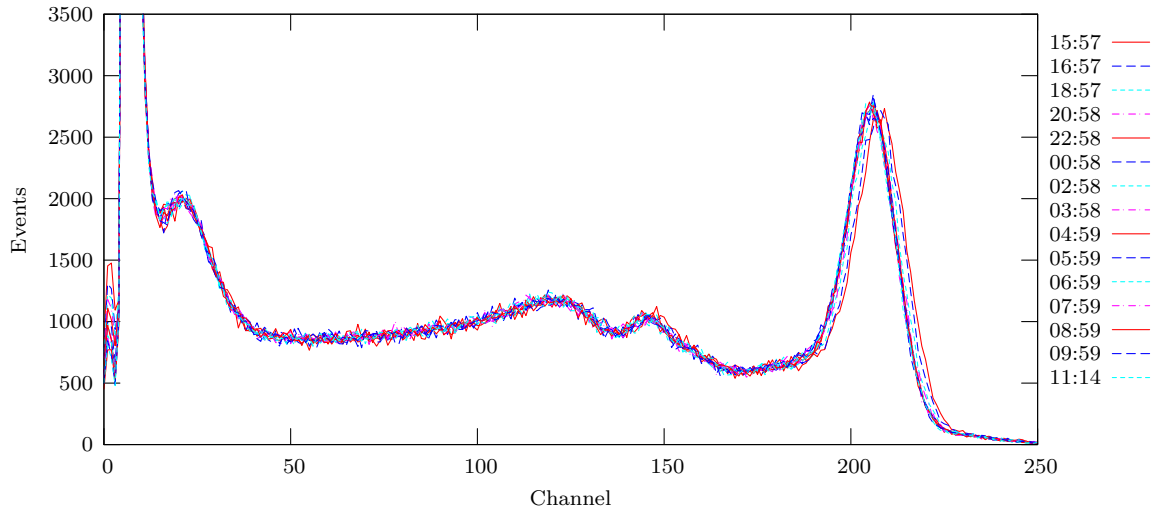


Figure 4.11.: Drift-Test without external magnetic field. After an usual start-up drift, the Bi-207 spectrum acquired with the PMT 9214SB stays constant for several hours.

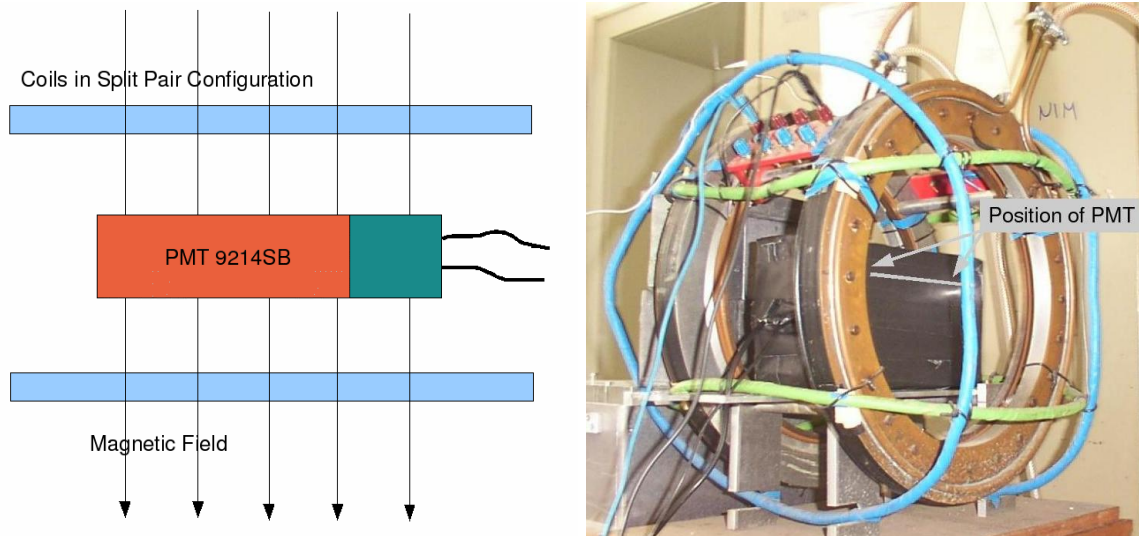


Figure 4.12.: Setup with perpendicular magnetic field.

Operation in perpendicular magnetic field

The PMT was placed inside an additional mu-metal shield MS52C (also by Electron Tubes). It was put between two coils in split pair configuration to produce a perpendicular magnetic field, see figure 4.12.

First the PMT was operated for almost 4 hours with no external field but the field of the earth. Then the magnetic field was increased up to 10 mT. As shown in figure 4.13, with

the increase of the magnetic field the count rate dropped rapidly. Additionally, an hysteresis effect occurred, since the gain is lower after the test than before (right picture in figure 4.13).

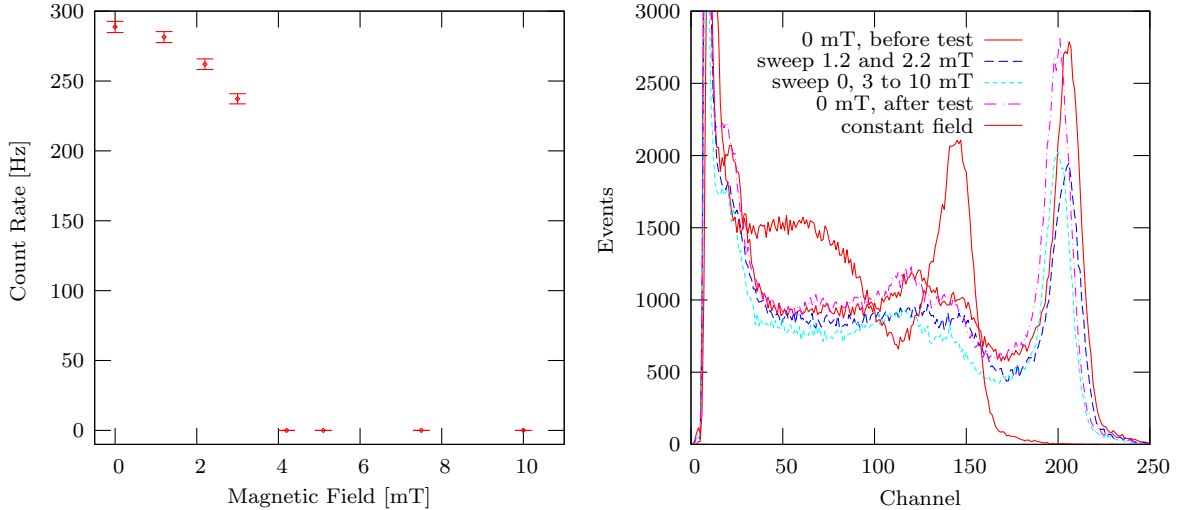


Figure 4.13.: Test of the PMT 9214SB in perpendicular magnetic field. The count rate drops rapidly with increasing magnetic field (left picture). The right graph shows the undesired change of the Bi-207 spectrum with different magnetic fields.

Test with parallel magnetic field

Although this setup is not needed for PERKEO III, we tested the behavior of the PMT parallel to the magnetic field. The result is shown in 4.14. Again, the count rate decreased rapidly and the PMT showed an hysteresis: The gain was slightly higher after the test with the magnetic field.

Summary

As an alternative to our existing PMTs by HAMATSU we tested the PMT 9214SB by Electron Tubes with an higher quantum efficiency compared to our standard Mesh-PMTs. Without any external field, there were no drifts in the gain of the PMT 9214SB. With an applied external magnetic field, the performance of the PMT gets worse and in fields greater than 3 mT it does not work at all.

Since the PMT 9214SB does not work properly in a magnetic field it is not sufficient for our purpose.

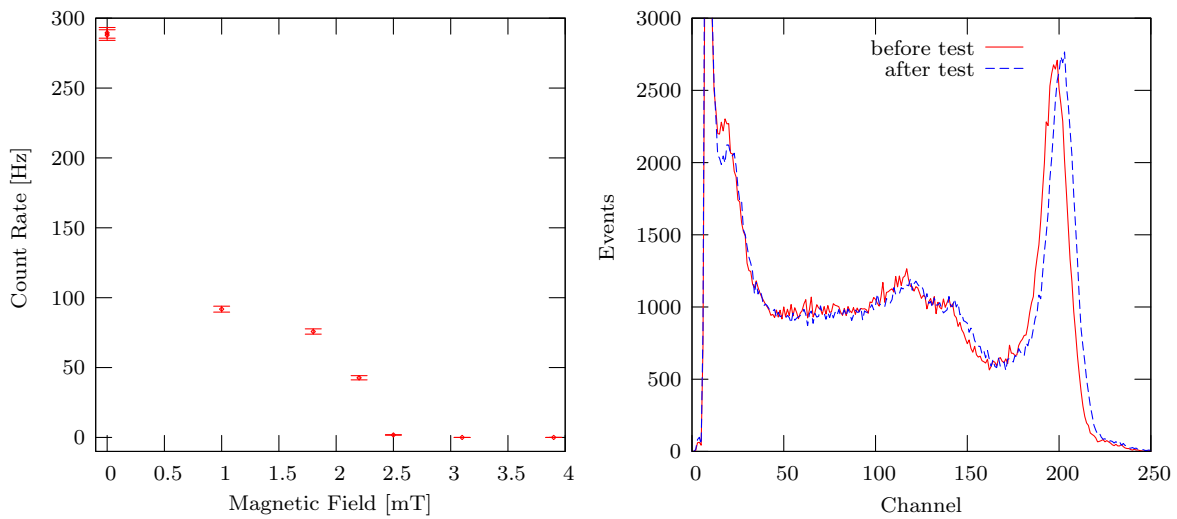


Figure 4.14.: Test of the PMT 9214SB in parallel magnetic field. The count rate drops with increasing field (left). On the right the Bi-207 is shown, measured before a applying a 3 mT field and afterwards. One can clearly see an hysteresis effect.

5. First Beamtime

In this chapter our measurements during the first beamtime at the cold neutron beam position PF1b at the ILL are presented. The ILL (Institut Laue-Langevin) in Grenoble, France, operates the European Neutron Source, an high flux reactor with a thermal power of 58.3 MW optimized for neutron production.

5.1. Beam Direction

To install the spectrometer and the beamline at the beam position, it is necessary to know the beam direction. Hence we had to determine the position of the beam maximum at the end of the experimental zone wherefore we used a ^3He -detector with 3% efficiency and $2 \times 2 \text{ cm}^2$ window, movable in horizontal (x) and vertical (y) direction, both perpendicular to the beam.

Direct beam

First we determined the direction of the neutron beam without polarizer or any other attenuation. This measurement was necessary since the wall at the end of the PF1b zone was shifted for PERKEO III by 1.5 meters; of course, the mark on the wall indicating the beam direction was lost.

An orifice (1 mm in diameter) was fixed behind the exit of the neutron guide. We determined the maximum of the beam intensity in x and y -direction at the end of the zone. In x -direction, see figure 5.1, the beam profile showed an asymmetric structure due to the characteristics of the neutron guide, cf. [Mun00]. The origin of the small peaks at $x = 500 \text{ mm}$ and $x = 750 \text{ mm}$ is unknown, maybe due to damages in the guide.

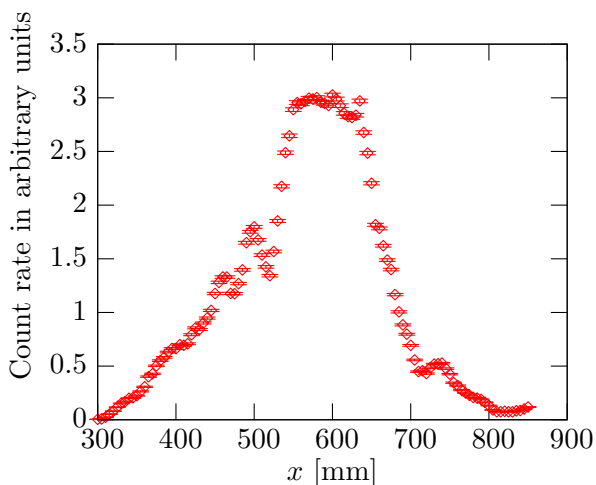


Figure 5.1.: Profile in x -direction of the direct neutron beam without polarizer or any other attenuation, measured at the position of maximal vertical (y) intensity. One can see an asymmetric structure which is due to the neutron guide geometry. The origin of the smaller peaks is unknown but not critical for the PERKEO III measurement.

Polarized beam

To measure the weak magnetism form factor we need a beam of polarized neutrons. Hence a polarizer was installed directly behind the neutron guide exit. However, this deflects the neutron beam and we had to determine the beam direction again. First, the polarizer was adjusted to gain maximum polarization by varying its angle relative to the beam.

Then we determined the beam profile with the polarizer. This time a small orifice of 5mm diameter at the polarizer exit was used. The measured profiles are shown in figures 5.2. In both graphs, there is only one single peak visible, what is interesting since in some former measurements two or four peaks occurred. We determined the beam position at the end of the experimental zone from the maximum beam intensity in x and y -direction; this position then was used for the alignment of the beamline and the PERKEO III instrument.

Attenuated beam

In former experiments beam direction measurements were often done using plexiglass sheets to attenuate the neutron beam for radioprotection reasons. However, it was unclear how the attenuator influences the results of the measurement. Therefore we determined the beam position with a 10 mm plexiglas attenuator installed in front of the polarizer. As one can see in figure 5.3 the width of the peak decreases and the maximum is slightly shifted in the attenuated measurement. Due to the decreased intensity in the attenuated case, data is scaled for comparison. The shift of the maximum in x -direction is only a very small effect (7 mm) related to the distance between polarizer and detector (approximately 12 m).

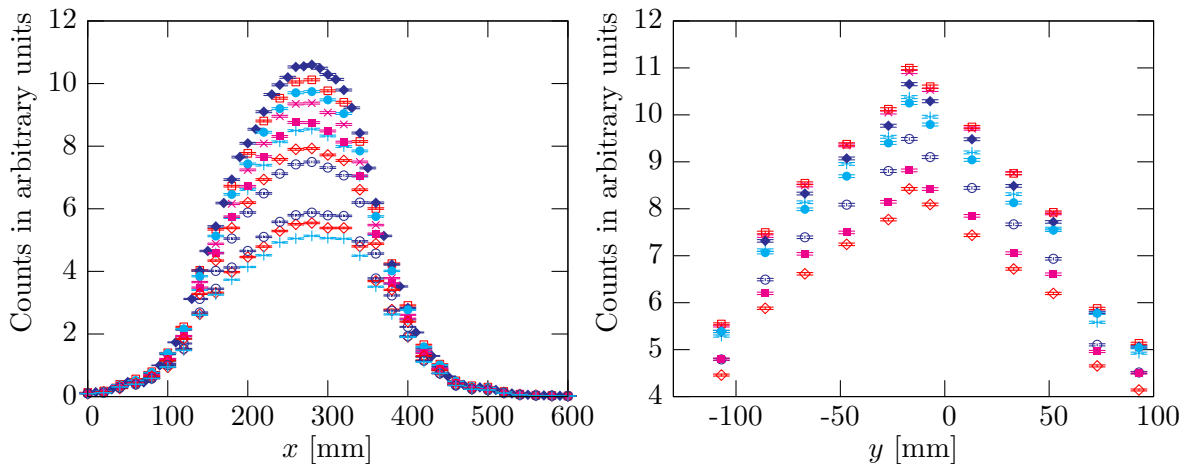


Figure 5.2.: Beam profiles with polarizer measured at the end of the experimental zone. Left: x -profile at different y -heights (spacing 20 mm) Right: y -profile at different x -positions (spacing 20 mm). The profiles are much more symmetric and show less structure than figure 5.1 since a larger orifice was used and the polarizer changes the beam divergence.

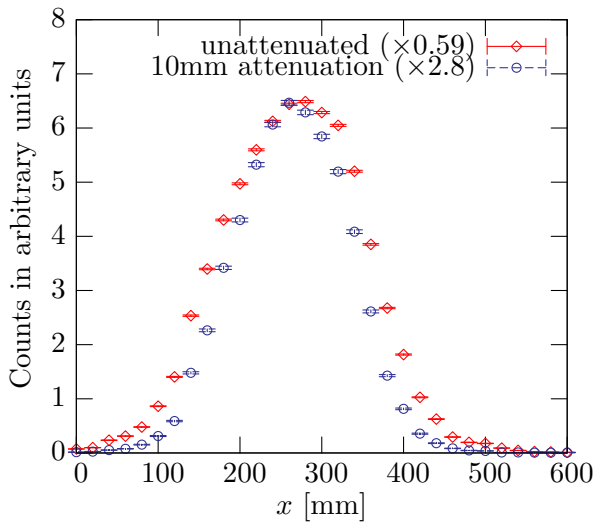


Figure 5.3.: x -profile of the neutron beam with and without attenuator between neutron guide exit and polarizer. Data is scaled to allow comparison. The peak width of the attenuated measurement decreases and the maximum is shifted slightly.

5.2. Background Measurements

The following measurements have all been done without a magnetic field. Hence no electrons from the decay volume can reach the detectors, even in measurements with neutrons.

Initial Startup of Photomultipliers

The photomultipliers were switched on for the first time at normal pressure (approx. 1 bar) in complete darkness, since all vessels of PERKEO were closed. We made a crude calibration using a monoenergetic ^{207}Bi conversion electron source with an electron decay rate $r \approx 1$ kBq. The source was fixed at the center of the scintillator. Each detector was calibrated separately, i.e. the other one only measured background. For both detectors we determined the positions of the pedestal, i.e. the ADC entry when no signal is applied, and the upper peak of ^{207}Bi at approximately 1 MeV. They were used to obtain a crude energy-channel calibration for each detector. The approximate error of $\pm 15\%$ is estimated because the pedestal is not exactly at zero energy due to detector non-linearities at very low energies, and we only have one single peak with known energy since the lower ^{207}Bi -peak is not visible due to the large γ -background of the source. The final calibration will be done with six different electron peaks, cf. [Wil07].

Shielding of Detector 1

Minimizing the background in the data is a crucial task for precision measurements. To get an estimation of the background count rate in the experiment, the effect of a 10 cm Pb plate covering the front of detector 1 was examined. The setup is sketched in the right part of figure 5.4 and table 5.1 shows the resulting count rates of both detectors measured under different conditions. The contents of the first two rows are the background rates without neutron beam which is due to surrounding experiments and neutron guides. One can see that the Pb plate reduces the background count rate in detector 1 by only 13%. Next we turned on the neutron beam which increased the background at detector 1 by roughly 1 kHz and about 2.5 kHz at detector 2 (compare row 2 to row 3). The high background at detector 2 is due to the unshielded beam stop just below it (see fig. 2.2). The increased background at detector 1 is produced by the collimation system consisting of four apertures (ref. [Wil07]).

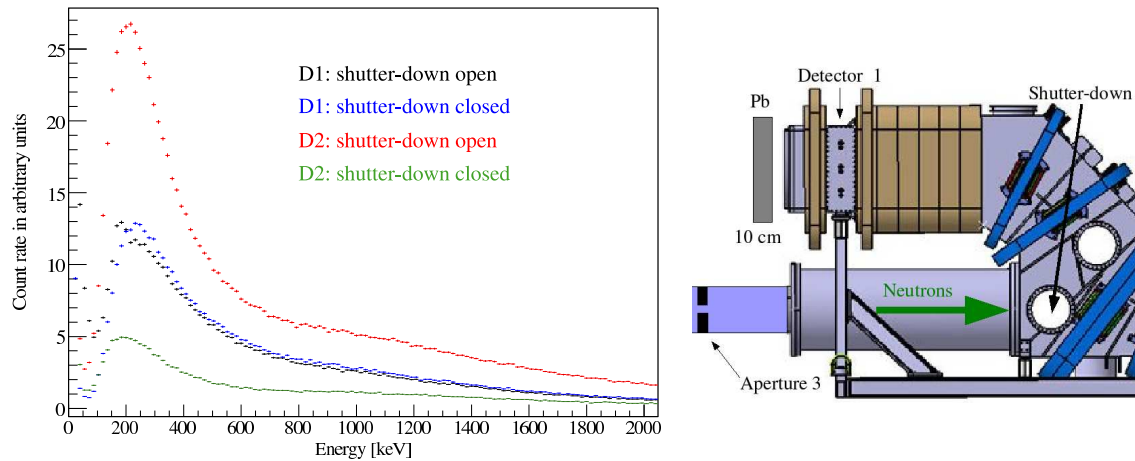


Figure 5.4.: The plot on the left shows spectra measured with the Pb plate in front of detector 1. The corresponding trigger rates are shown table 5.1, row 3 and 4. Most of the background has an energy below 400 keV. The big difference in the detector 2 rates is due to the large effect of the beamstop, that only occurs when the shutter is open. On the right, the setup with the 10 cm Pb plate is shown.

Aperture 3 for example produces around 300 Hz, what can be seen by comparing rows 3 and 4 with rows 7 and 8 respectively. The closed shutter-down produces a background of 220 Hz on detector 1, which is the difference of the values in row 4 and 3, as well as row 8 and 7.

One can also see that detector 2 is not influenced by the shielding of aperture 3 and the rest of the collimation system because of its distance (≈ 8 m).

Beam	Shielding	Shutter-up	Shutter-down	D1 [Hz]	D2 [Hz]
off	none	open	open	415	520
off	Pb-plate D1	open	open	360	520
on	Pb-plate D1	open	open	1380	3050
on	Pb-plate D1	open	closed	1600	580
on	none	open	open	2800	3040
on	none	open	closed	2960	600
on	Pb-plate D1 ^a	open	open	1680	3070
on	Pb-plate D1 ^a	open	closed	1900	600

^aThe shielding (some Pb bricks) at aperture 3 was removed.

Table 5.1.: Influence of shielding on the background count rate measured in different setups. The two rightmost columns contain the average count rates of the two detectors. Column 3 indicates whether the Pb plate (see figure 5.4) was placed in front of detector 1. By calculating the differences of the several count rates one can obtain the effects of the different configurations. This is discussed in the text.

Shielding of Detector 2

The background of detector 2 was investigated without neutron beam using again a 10 cm thick Pb plate. Two positions of the Pb plate were tested, behind detector 2 and next to it; in Figure 5.5 both configurations are shown in the picture on the right. The plot on the left shows three spectra: one without any shielding and one for each position of the plate. One can see that in the setup with the plate next to the detector the shielding has no significant effect. This is interesting since a neutron guide is installed behind the wall next to PERKEO III producing much background radiation (up to $16 \mu\text{Sv/h}$) that might disturb the measurements. Maybe the shielding with the lead plate was not sufficient since the guide emits radiation over the whole length of the experiment.

The form of the background spectra is similar to detector 1. The Pb plate behind detector 2 decreases the count rate also by roughly 13%. But in this case the background sources are different: It is mainly due to the experiments directly behind our setup.

Shielding of the Beamstop

As expected, our measurements showed that a significant number of neutrons are scattered at the ${}^6\text{LiF}$ -beamstop and escape from there. To suppress their effect on the background they have to be shielded with boron. Therefore a cage made out of borated aluminium (*boral*) will be built around the beam stop. In former measurements similar shieldings were used, cf. [Sch04, Mun06].

Background from the Beamline

Background produced by neutrons in the beamline is crucial since it is beam related, i.e. it only occurs when shutter-up is open. Therefore tons of lead suppressing the radiation have to be installed around the beamline. To optimize this, several positions along the unshielded beamline have been investigated for γ and neutron radiation. The first was measured with the *Rados* detector, a simple γ -counter available at the beam position, and the neutrons with

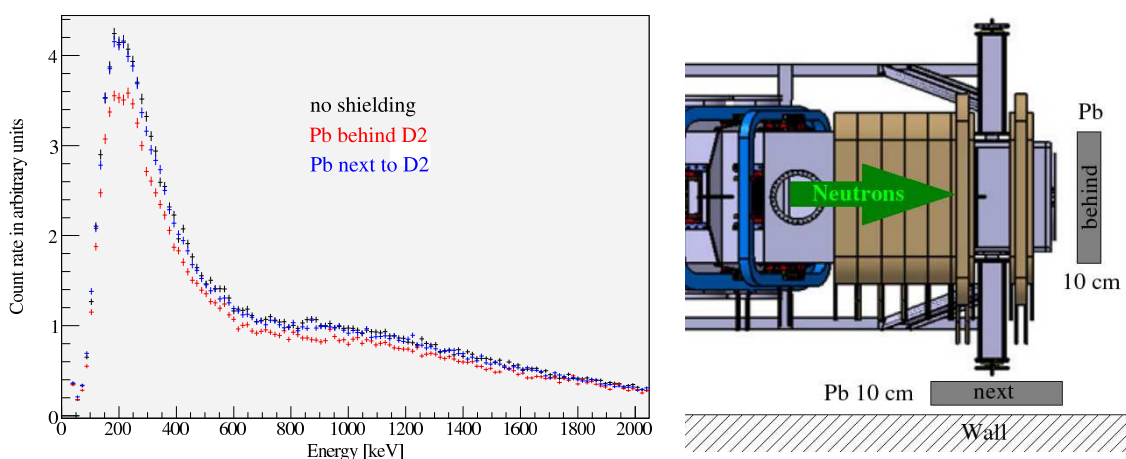


Figure 5.5.: Left: Three spectra acquired with detector 2 in different configurations are shown. The spectra are similar to detector 1. On the right the configuration is sketched. However, shielding detector 2 is difficult.

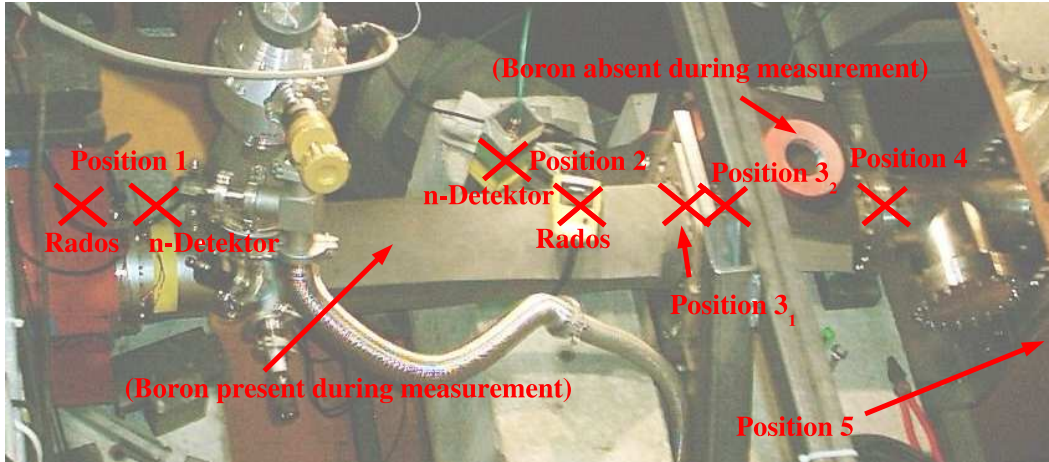


Figure 5.6.: The positions to identify the neutron and γ -background sources along the beam-line. Position 5 is located 30 cm in front of the last aperture and shutter down; the neutron counter was placed 40 cm above the beam, the γ -counter 80 cm below.

Position	Beam	Shutter-up	γ [$\mu\text{Sv/h}$]	n [1/10 s]
1	off	closed	0.6	1
	on	closed	40.0	20
	on	open	57.0	290
2	off	closed	1.6	1
	on	closed	40.0	5
	on	open	110.0	235
3 ₁	off	closed	2.0 ^a	1
3 ₂	on	closed	30.5 ^a	9
3 ₁	on	open	22.0 ^a	180
4	off	closed	1.5	1
	on	closed	16.5	4
	on	open	25.9	184
5	off	closed	2.2	2
	on	closed	2.3	3
	on	open	4.4	103

^aThe Positions of the gamma measurements were not exactly the same. This is indicated by the subscripts in the first column, see also figure 5.6

Table 5.2.: Count rates for γ -photons and neutrons at different positions along the beam line.

a ^3He counter. Figure 5.6 indicates the different measuring positions, aperture 3 (mentioned above) is inside the tube at position 2 of the Rados in the picture. For the investigations, we removed its Pb brick shielding (corresponding to the measurements in row 7 and 8 in table 5.1). Table 5.2 shows the count rates at the different positions without beam and with either of the shutters closed. One can see that aperture 3 produces much γ -radiation which agrees with the shielding measurements above.

Background from adjacent experiments

Long time measurements of the background show structures in the count rates that are caused by experiments in the neighborhood of the PF1b beam position. By using data from INESS¹ it is possible to identify some of the experiments causing this structures. This is very important since we later have to select data with constant background, and because wrong determined background is one of the most important sources of systematic errors.

Figure 5.7 shows the background signal of both detectors and the shutter states of the neighboring experiments D1B² and IN11³. One can see that D1B only influences detector 2, which is much closer to the diffractometer, whereas IN11 has a significant effect on both detectors.

From the data shown in figure 5.7 lower limits for the signal-to-noise ratio of roughly 5.5:1 for detector 1 and 8.8:1 for detector 2 were obtained, assuming a total neutron decay rate of 30 kHz. It is only a lower limit since the test was done without any proper shielding of beamline and detectors.

¹Service at the ILL providing the shutter status for all experiments and neutron guides.

²A high intensity powder diffractometer [D1B]

³Spin-Echo Spectrometer IN11 [IN11]

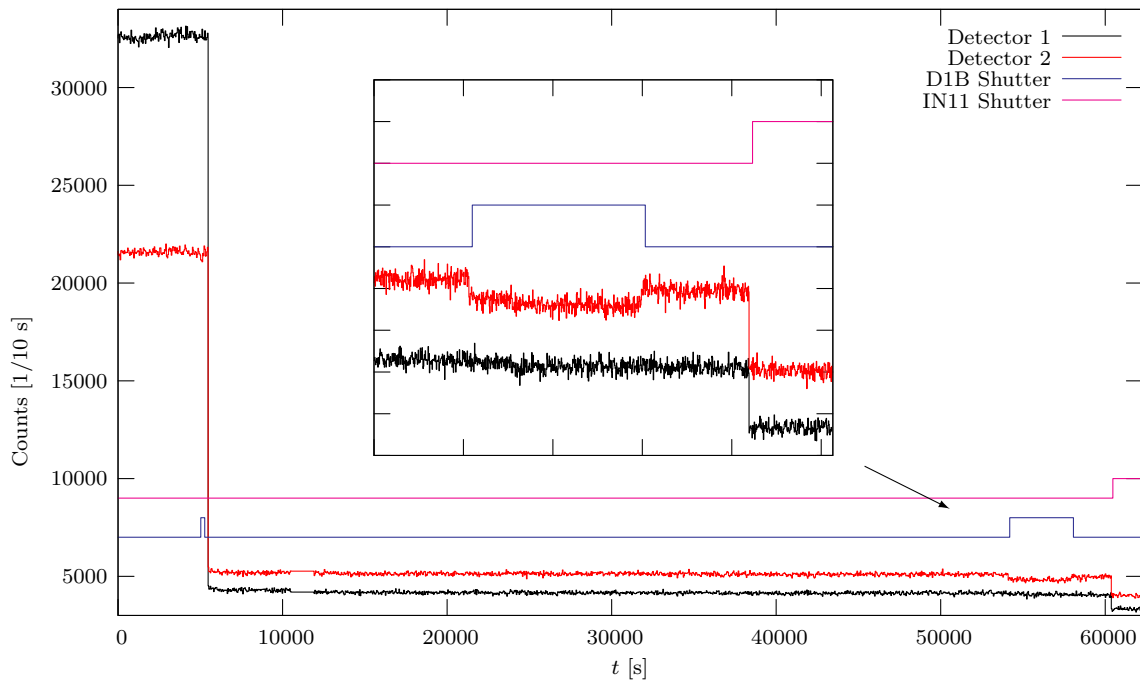


Figure 5.7.: Effect of the adjacent experiments D1B and IN11 on the background count rate of the detectors. In the first 5000 seconds the neutron beam was on, then it was switched off and only the background of the experimental hall was measured. One can clearly identify the jumps in the count rates due to D1B and IN11. Whereas the latter can be seen in both detectors, D1B only causes an effect in detector 2.

6. Summary

Neutrons are an ideal object to perform precise tests of the theory of weak interaction. The weak magnetism, a small contribution in the generalized decay matrix element accounting also for other interaction than vector V and axialvector A , can be extracted from a energy dependence of the β asymmetry A of free neutron decay. It is a very small effect in the order of 1%. Previously this parameter was not accessible in neutron decay due to limited statistics. The new spectrometer PERKEO III is the first instrument that will achieve a neutron decay rate large enough to measure this parameter with the necessary precision.

The aim of this thesis was the preparation of the first measurement with the new instrument. It was built up at the cold neutron beam facility PF1B of the ILL.

As the first of the PERKEO instruments it uses normal conducting coils cooled with water. The high electrical power necessary to generate the magnetic field and the large number of coil segments require a complex cooling system with high water flow. This has been developed within the scope of this thesis, and the flows in the subcirculations have been calculated to dimension single parts of the cooling system. A heat exchanger was installed and connected to PERKEO and the cooling circulations at the ILL. Measurements were made to check if the heat dissipation is sufficient and the results approved that the dimensioning is correct and that the cooling system works reliable. For safety reasons, a waterflow watchdog has been developed that is able to monitor the different flows in the subcirculations and to turn off all critical devices in case of a failure.

For the data acquisition system the electronics of PERKEO II is largely reused. The expected decay rate of approximate 30 kHz is two magnitudes higher than in previous experiments and made the acceleration of the data acquisition system necessary. To achieve this, the hardware had to be upgraded and a new readout software was written from scratch. The system is now able to cope with a data rate that is 100 time higher than the data rate of the last PERKEO II experiments. In the process of building up the electronics, the linearity of the used ADCs has been studied and was improved significantly.

During the first beamtime in winter 2006, first measurements were made on the beam direction to align the spectrometer. Furthermore we started detailed studies on the beam related background and shielding possibilities. The influence of adjacent experiments on the background was examined.

A. Time measurement in Linux using the TSC

To determine and optimize the data transfer rate from the VME devices, exact time measurements are necessary. In a multitasking environment this is a little tricky, since several programs share the resources of the computer at the same time. In this appendix first is shown how the turning-off of the clock interrupt disturbed our the measurements and why the results are wrong. Then a way how to do it right is shown. This will be useful for further acceleration of the data acquisition or general purpose time measurements in Linux.

Our first approach to measure the data rate was by using the POSIX¹ `clock()` function, shown in listing A.1. The constant `CLOCKS_PER_SEC` equals 1000000, hence on a 32-bit system the function returns the same value every 72 minutes. The problem of this method are wrong results if the clock interrupt is turned off during the measurement. This gives a far to low time difference, which leads to the wrong results. This is the case for the SIS3100/1100 DMA transfers invoked by `vme_A32DMA_D32FIFO_read()`, see figure A.1. The average time per request and the data rate are completely unrealistic for this function.

```
t1 = clock          //save time before action

action();          //do action to measure

t2 = clock();      //save time after action

//calculate the difference and scale it to seconds
dt = (t2-t1) / CLOCKS_PER_SEC;
```

Listing A.1: First approach to measure the data rate of the VME system.

To get proper results one has to use a different method. Most modern processors have an internal register counting the CPU cycles, it is called Time Stamp Counter (TSC). This counter is incremented on every cycle the CPU does. Our system has CPU frequency of 1.6 GHz, so we achieve a resolution of 0.625 ns.

The TSC method also has some problems:

- To calculate a measured time value the CPU frequency has to be known.
- On some modern processors, the frequency is not constant to save energy.
- A 32-bit wide TSC overflows in few seconds for CPU frequency in the order of 1 GHz.
- The read out of a 64-bit TSC is not possible as a single access, but may not be interrupted for correct measurement.

In our 32-bit Linux environment the TSC can be read out via the macro `rdtsc()`, ref [Rub02]. The macro takes care that no interruption occurs during read out of the 64-bit

¹Portable Operating System Interface for uniX - a family of standards by the IEEE for compatibility with Unix operating systems.

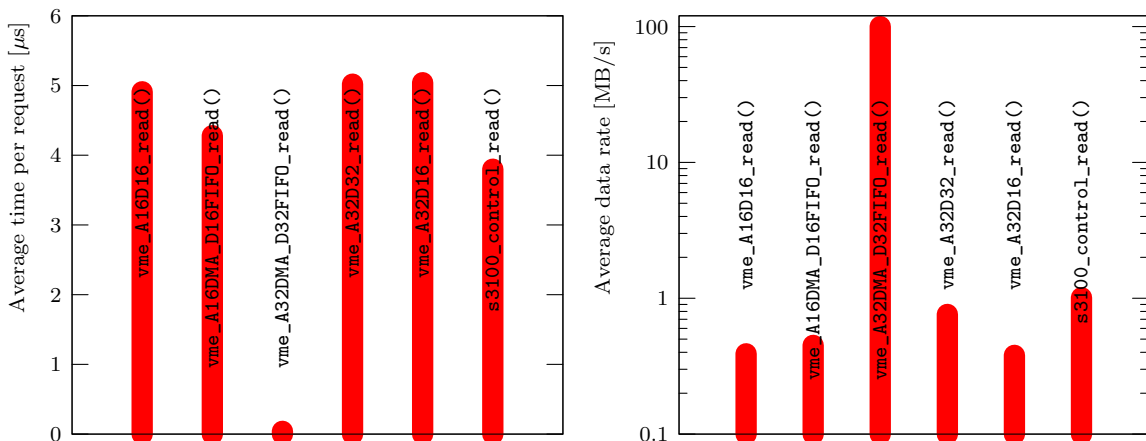


Figure A.1.: First time measurements for different requests to the VME Bus using the SIS3100/1100 PCI to VME link. The values for `vme_A32DMA_D32FIFO_read()` are wrong. This can be seen from the unrealistic values for request duration and data range (the standard VME bus is maximally capable of 40 MB/s data rate). The timer interrupt used for the measurements is turned off during DMA-accesses to the PCI bus. This gives far to low time differences and leads to the wrong results.

TSC. We can easily figure out the cpu frequency, which is constant for our system. A work-around for a non-constant cpu frequency is given in [Kun06]. We developed some macros that make the time measurements very easy:

- `TM_INIT()` figures out the cpu frequency and has to be called only once in the program.
- `TM_START()` must be called just before the action to measure starts.
- `TM_STOP()` ends the measurement. It handles possible overflows and calculates the time elapsed.

Listing A.2 shows the source code of the macros:

```
#ifndef timemeasure_h
#define timemeasure_h

#include <stdlib.h>
#include <string.h>
#include <stdio.h>

#include <asm/msr.h>

#ifdef __cplusplus
extern "C" {
#endif

u_int32_t tm_cpu_freq;
```

```
u_int32_t tm_ini_h, tm_ini_l, tm_end_h, tm_end_l;
u_int64_t tm_delta;
double    tm_secs;

int TM_INIT() //just get cpu frequency
{
    FILE *fp;
    int bufsize = 1024;
    char buf[bufsize];
    double freq;

    if(!(fp=fopen("/proc/cpuinfo","r"))) return -1;

    while(!feof(fp)) {
        fgets(buf,bufsize,fp);

        if(strstr(buf,"cpu MHz"))
        {
            sscanf(buf,"cpu MHz : %lf",&freq);
            tm_cpu_freq = (u_int32_t)(freq*1e6);
            return 0;
        }
    }

    fclose(fp);
    return -1;
}

#define TM_START()  rdtsc(tm_ini_l,tm_ini_h)
#define TM_STOP()  { rdtsc(tm_end_l,tm_end_h);\
                    tm_delta=( ((u_int64_t)tm_end_h)<<32 |
                                tm_end_l)\
                                -(((u_int64_t)tm_ini_h)<<32 |
                                  tm_ini_l));\
                    tm_secs=((double)tm_delta) / tm_cpu_freq; }

#ifdef __cplusplus
}
#endif
#endif
```

Listing A.2: C-language include file containing macros for time measurements in Linux with TSC register.

An example for usage of the macros define above is given in listing A.3

```
#include "timemeasure.h"

int main(int argc, char *argv[])
{
    int i,j,k;
    double mean=0;

    if( TM_INIT() ) return -1; //error on init, exit program

    for(k=0; k<10000; k++) {
        TM_START();
        for(i=0; i<100; i++)
            j=i*i;
        TM_STOP();

        mean += tm_secs * 1000;
    }
    printf("cpu frequency = %d [Hz]\n\n"
           "the action took %g [ms]\n\n", tm_cpu_freq,
           mean/10000);

    return 0;
}
```

Listing A.3: Example how to use the macros for a time measurement. The first 100 square number are calculated. To increase the accuracy, the measurement is repeated 10000 times.

Bibliography

- [Abe02] H. Abele et al., Phys. Rev. Let. 88 (2002) 21
- [BC400] Data sheet for Bicron BC400 Premium Plastic Scintillators, available from <http://www.detectors.saint-gobain.com>
- [Bre03] A. Brehm, Praktikum der Technischen Chemie, Strömungslehre, 2003
<http://www.uni-oldenburg.de/tchemie/Praktikum/Stroemungslehre.pdf>
- [Cae01] CAEN: Technical Information Manual TDC V767A, 2001 <http://www.caen.it/getattach.php?mod=V767A&obj=mn>
- [Dackel] Dackel source code available from: <http://www.physi.uni-heidelberg.de/~kaplan/dackel>
- [D1B] High intensity powder diffractometer D1B at ILL, <http://www.ill.fr/YellowBook/D1B/>
- [Ger77] H.Vogel, Gerthsen Physik, z.B. 13. Auflage, 1977
- [IN11] Spin-Echo Spectrometer IN11, <http://www.ill.fr/YellowBook/IN11/>
- [Jac57] J.Jackson, S.Treiman and H.Wyld, Jr.: Possible Tests of Time Reversal Invariance in Beta Decay. In: Phys. Rev., 106 (1957) 517-521.
- [Kun06] Kunst, Quade: "Kerntechnik", Folge 27, Linux Magazin 04/06, S.118
<http://www.linux-magazin.de/Service/Books/Buecher/HW-Treiber/book1.html>
- [Kre04] M. Kreuz: Messung von Winkelkorrelationen im Zerfall polarisierter Neutronen mit dem Spektrometer PERKEO II, Ph.D. thesis 2004
- [Kre05] M. Kreuz, Phys. Lett. B 619 (2005) 263
- [Lab] Labcourse Computer Science, Kirchhoff Institute for Physics, Unit3: Basics of Analog Digital Converters, Manual
<http://www.kip.uni-heidelberg.de/ti/teaching/labcourse/unit3/>
- [Leo94] W.R. Leo, Techniques for Nuclear and Particle Physics Experiments, 2nd Edition, 1994
- [Mär06] B.Märkisch: Das Spektrometer Perkeo III und der Zerfall des freien Neutrons, Ph.D. thesis 2006
- [Mun00] D.Mund: Aufbau eines Experiments zur Messung der Neutrinoasymmetrie im Zerfall freier Neutronen, Dipl. thesis 2000
- [Mun06] D.Mund: Messung der Beta-Asymmetrie A im Neutronenzerfall, Ph.D. thesis 2006

- [Nis05] E.W. Lemmon, M.O. McLinden and D.G. Friend, "Thermophysical Properties of Fluid Systems" in NIST Chemistry WebBook, NIST Standard Reference Database Number 69, Eds. P.J. Linstrom and W.G. Mallard, June 2005, National Institute of Standards and Technology, Gaithersburg MD, 20899 (<http://webbook.nist.gov>).
- [Nom06] NOMAD: www.ill.fr/pages/science/User/pdf/NOMAD.pdf
- [Plo00] C.Plonka: Verbesserung der Lichtauskopplung zur Messung der Neutrinoasymetrie mit Perkeo II, dipl. thesis 2000
- [PMT9214SB] Data sheet for Electron Tubes PMT 9214SB, <http://www.electrontubes.com/pdf/9214B.pdf>
- [Rei99] J.Reich: Winkelkorrelationen im Zerfall polarisierter Neutronen, Ph.D. thesis 1999
- [Root] ROOT: An object-oriented data analysis framework developed at CERN <http://root.cern.ch>
- [Rub02] Rubini, Corbert: Linux-Gerätetreiber, Kapitel 3, 2. Auflage, 2002
- [Sch04] M.Schumann: Probing the Standard Model: Preparation of a new Electron Asymetry Measurement in the Decay of Polarized Neutrons, Diploma thesis 2004
- [Sch07] M.Schumann: Ph.D. thesis in progress 2007
- [Sta01] W. Stallings: Operating Systems, 2001
- [Stö00] H.Stöcker: Taschenbuch der Physik, 4. Auflage, 2000
- [Sol02] T.Soldner, A.Petoukhov, C.Plonka: Installation and first tests of the new PF1b polariser, 2002
- [Wil82] D. H. Wilkinson: Analysis of neutron β -decay. In: Nuclear Physics A, 337 (1982) 474-504
- [Wil07] D.Wilkin: Diploma thesis in progress, 2007
- [Wik06] Wikipedia: picture of a signal in a constant fraction discriminator.
- [zlib] zlib general purpose compression library <http://www.zlib.net/>

Erklärung:

Ich versichere, dass ich diese Arbeit selbständig verfasst und keine anderen als die angegebenen Quellen und Hilfsmittel benutzt habe.

Heidelberg, den 12. Januar 2007